AD_____

Award Number: W81XWH-04-1-0262

TITLE: Targeting MRS-Defined Dominant Intraprostatic Lesions with
Inverse-Planned High Dose Rate Brachytherapy

PRINCIPAL INVESTIGATOR: Jean Pouliot, Ph.D.
I-Chow Hsu, M.D.
John Kurhanewicz, Ph.D.
Sue Noworelski, Ph.D.

CONTRACTING ORGANIZATION: University of California, San Francisco
San Francisco, CA 94143-0962

REPORT DATE: February 2005

TYPE OF REPORT: Annual

PREPARED FOR: U.S. Army Medical Research and Materiel Command
Fort Detrick, Maryland 21702-5012

DISTRIBUTION STATEMENT: Approved for Public Release;
Distribution Unlimited

The views, opinions and/or findings contained in this report are those
of the author(s) and should not be construed as an official Department
of the Army position, policy or decision unless so designated by other
documentation.

20060525018

REPORT DOCUMENTATION PAGE

1. AGENCY USE ONLY (Leave blank)	2. REPORT DATE February 2005	3. REPORT TYPE AND DATES COVERED Annual (26 Jan 2004 – 25 Jan 2005)

4. TITLE AND SUBTITLE
Targeting MRS-Defined Dominant Intraprostatic Lesions with Inverse-Planned High Dose Rate Brachytherapy

5. FUNDING NUMBERS
W81XWH-04-1-0262

6. AUTHOR(S)
Jean Pouliot, Ph.D.
I-Chow Hsu, M.D.
John Kurhanewicz, Ph.D.
Sue Noworelski, Ph.D.

7. PERFORMING ORGANIZATION NAME(S) AND ADDRESS(ES)
University of California,
San Francisco
San Francisco, CA 94143-0962

E-Mail: pouliot@radonc17.ucsf.edu

8. PERFORMING ORGANIZATION REPORT NUMBER

9. SPONSORING / MONITORING AGENCY NAME(S) AND ADDRESS(ES)
U.S. Army Medical Research and Materiel Command
Fort Detrick, Maryland 21702-5012

10. SPONSORING / MONITORING AGENCY REPORT NUMBER

11. SUPPLEMENTARY NOTES

12a. DISTRIBUTION / AVAILABILITY STATEMENT
Approved for Public Release; Distribution Unlimited

12b. DISTRIBUTION CODE

13. ABSTRACT (Maximum 200 Words)
During this first year, we have obtained CHR approval (December 2004) from the three step process (G.U., P.R.C. and C.H.R.) committees at UCSF. Patient enrollment will begin immediately after receiving CHR approval from D.O.D. The accuracy of aligning MRI/MSRI data acquired with different types of endorectal probes to images acquired without a probe was determined. A 94% Average overlap of prostate contours was obtained using rigid endorectal coil. We have also obtained a class solution for the boost of DIL defined by MRI/MRSI and the maximum achievable boost level under clinical dosimetric requirements using data from 10 previously treated HDR brachytherapy patients.

14. SUBJECT TERMS
Magnetic resonance spectroscopy, inverse planning HDR brachytherapy

15. NUMBER OF PAGES
58

16. PRICE CODE

17. SECURITY CLASSIFICATION OF REPORT	18. SECURITY CLASSIFICATION OF THIS PAGE	19. SECURITY CLASSIFICATION OF ABSTRACT	20. LIMITATION OF ABSTRACT
Unclassified	Unclassified	Unclassified	Unlimited

PC030909 Annual Progress Report
January 2004 – January 2005

Contact information:

Jean Pouliot, Ph.D.
Professor
Department of Radiation Oncology
UCSF Comprehensive Cancer Center
1600 Divisadero Street, Suite H1031
San Francisco, Ca-94143-1708
Tel: 415 353-7190
Fax: 415 353-9883
E-mail: pouliot@radonc17.ucsf.edu

Table of Contents

INTRODUCTION

Research Project Description

Recent developments in high spatial resolution Magnetic Resonance Imaging (MRI) and Magnetic Resonance Spectroscopic Imaging (MRSI) from UCSF have significantly improved the ability to identify regions of cancer within the prostate and to discriminate them from surrounding healthy tissues.

In this project, we propose a comprehensive, innovative approach that incorporates MRI/MRSI anatomic and metabolic information to guide the determination of the optimal dose distribution. First, in order to increase radiation to the tumor part of the prostate and to reduce radiation to normal structures, these regions must be reliably identified and delineated in the anatomical image used for the treatment plan. Second, determining such an individualized, complex, conformal radiation dose plan necessitates the use of an optimization algorithm.

Incorporating the MRI/MRSI information is currently difficult. The exam cannot be obtained at the time of the treatment planning MRI due to the need for an endorectal probe and due to artifacts from the catheters inserted for the treatment. To transfer the information from the MRI/MRSI to the treatment planning MRI, tissue distortions must be corrected and the data aligned.

Additionally, we propose to develop a novel high dose rate brachytherapy (HDR) planning protocol using a computerized optimization algorithm using multiple objectives to provide a boost while preserving nearby healthy tissues.

Three main tasks were identified to fulfill the aims of this project:

Task 1: To determine the need for alignment and to establish alignment methods for MRI/MRSI data to HDR brachytherapy treatment planning MRI and CT images. (Months 1-24).

Task 2: To elaborate class solutions (a set of optimization constraints) appropriate for DIL boosts of the order of 150% of the prescribed dose and protection for the penile bulb and the neuro-vascular bundle valid for 90% of the cases (Months 1-12).

Task 3: To perform feasibility and short-term measures of improved effectiveness and decreased side effects of performing the proposed treatment planning protocol in a small cohort of patients (Months 18-36).

The Information provided in this first annual report supports the following:

Task 1:	Months 1-24	In progress
Task 2:	Months 1-12	In progress
Task 3:	Months 18-36	Not yet initiated

C.H.R. approval

The PC-030909 grant officially opened on February 2004. A lot of effort and time were devoted by the P.I. and Co-P.I. at applying and obtaining approval from the various committees at UCSF. During the first year, we sequentially applied and successfully received approvals from the UCSF Genito-Urinary Committee (GU, March 2004), the UCSF Protocol Review Committee (PRC, July 7th, 2004), and the UCSF Committee on Human Research (CHR, approval number H11386-24294-01, December 17th, 2004). Immediately after receiving the CHR approval, the complete package was submitted to the DOD CHR for final approval. This approval is pending. Patients enrollment will begin immediately when DOD approval is received.

Research activities

A number of research activities related to the Tasks described in the Statement of Work of the proposal where initiated during 2004. In particular, the first items of Task 1 and Task 2 have been accomplished. Specific details on each item are provided in the next section. A Postdoctoral Fellow (Yongbok Kim, Ph.D.) was enrolled in February 2004 to perform the work. The work was conducted mainly under the supervision of the Co-PI at the MRSI center.

In order to make progress as DOD Human Subjects Research Review Board (HSRRB) approval for the research is pending, we have retrospectively looked at MRI data already acquired and anonymized from a different study. This has allowed us to develop appropriate tools and come up to some conclusions as how to progress when DOD approval comes.

BODY SECTION

Preliminary work

In this study we were proposing a comprehensive approach that incorporates MRI/MRS's anatomical and functional imagining into the HDR brachytherapy treatment planning. Using the inverse planning program IPSA, we established that we can target regions with a higher tumor burden with higher dose without increasing the dose to critical normal structures. The results of this work, used as preliminary studies to support the actual proposal, were finalized and published in August 2004 (copy of the paper is attached in Appendices D1).

Endorectal coil probes for prostate MRI: Assessments of tissue distortions and image alignments

For HDR brachytherapy planning using the combined MRI/MRSI information, there are three confounding factors: (1) anatomical distortions due to the use of the ERC probe in the staging MRI/MRSI exam which is not used for the treatment planning CT or MRI exam, (2) the anatomical distortions caused by the placement of the catheters used for HDR brachytherapy, and (3) the alignment of the combined MRI/MRSI information to the actual treatment procedure. The expandable balloon-inflated endorectal coil (ERC) probe, produced by MedRad, Inc., has been the only commercially available and is therefore currently being used for prostate MRI/MRSI exams. The balloon on the ERC probe allows the coil to seat itself on the surface of the prostate. It also reduces peristaltic motion. However, the probe introduces a large air-tissue interface causing magnetic field susceptibility problems, which degrades the MR data quality.

More recently a rigid ERC (USA Instruments, Aurora, OH) has been developed and soon will be commercially available. In 2004, we have conducted a study (Task 1 of the proposal) [Kim-2005] (1) to investigate the change of prostate position and shape caused by the balloon-inflated ERC probe and by the rigid ERC probe, (2) to determine which ERC probe would produce less prostate deformation, (3) to assess manual rigid-body image registration between the diagnostic MRI scanned with the ERC probe and an MRI scanned without an ERC probe, and (4) finally to decide which ERC probe provides the best results for the registration of the MRI acquired with an ERC probe to that acquired without one. In this study, the prostate changes due to the ERC probe were investigated, thus providing preliminary data for the practical image registration applicable to the clinic.

Sagittal and axial T_2 weighted MR images were acquired from 20 patients receiving a combined MRI/MRSI staging exam for prostate cancer. Within the same exam, images were acquired using an external pelvic phased array coil both alone and in combination with either an expandable ERC or a rigid ERC. Rotations, translations and deformations caused by the ERC were measured and compared. The ability to register images acquired with and without the ERC using a manual rigid-body registration was assessed using a similarity index (SI). Both ERCs caused the prostate to tilt anteriorly with an average tilt of 19.4 degrees

5

(19.2 ± 13.4 and 19.5 ± 11.3 degrees, mean ± standard deviation, for expandable and rigid ERC, respectively). However, the expandable coil caused a significantly ($p < 0.05$) larger distortion of the prostate as compared to the rigid coil; compressing the prostate in the anterior/posterior direction by 4.7 ± 3.7 mm versus 1.2 ± 2.2 mm (14.1% versus 3.9%), and widening the prostate in the right/left direction by 6.1 ± 2.8 mm versus 1.5 ± 3.1 mm (16.7% versus 4.2%). Additionally, the ability to align prostate images acquired with and without ERC was significantly ($p < 0.0001$) better for the rigid coil (SI = 0.88 ± 0.04 versus 0.94 ± 0.008, for the expandable and rigid coils, respectively). In conclusion, the alignment of prostate MRI/MRSI data acquired using an ERC with therapeutic planning MR images acquired without an ERC can be improved through the use of a rigid ERC.

Class solution for Inverse Planning

The second task of the proposal consists to elaborate the dose constraint set (class solution) for the boost of DILs defined by MRI/MRSI in HDR brachytherapy of the prostate cancer. Before we begin the proposed task, we investigated the maximum achievable boost level under the dosimetric requirement of RTOG0321 protocol which recently was initiated. This work is a preliminary study in order to perform the proposed task efficiently.

For 10 patients, DILs were manually contoured on HDR planning CT/MR images based on combined MRI/MRSI. A lesion containing at least 3 contiguous MRSI validated cancer voxels was called a DIL. The class solution of dose constraints, acceptable dose range and penalty values, were obtained from our previous clinical experience on inverse planning technique (IPSA). For each patient, six plans (one without-boost and 5 different levels of dose escalation to the DILs requesting a minimum of 110, 120, 130, 140 and 150% of the prescribed dose, respectively) were generated using IPSA. Dosimetric indices for each plan were computed and compared with the requirement of RTOG0321 protocol to determine the acceptable level of dose escalation.

Plans without boost satisfied all RTOG0321 requirements with average dose coverage of 92.1% to target (range from 90.6 to 93.8%). Four (B, C, D, and J) out of 10 patients prohibited any boost whereas a certain level of boost to the DILs was feasible for the rest of patients, minimum dose of 110% for patient E, 120% for patient H and I, 140% for patient A and F, and 150% for patient G, respectively. The violation of RTOG0321 protocol is rectal dose for 9 patients and bladder dose for patient C. The average benefit from maximum achievable boost for 6 patients is 1.1% increase of target coverage and 5% increase of V120 dose to DILs compared with a plan without boost.

Key Research Accomplishments

Endorectal coil probes for prostate MRI: Assessments of tissue distortions and image alignments

- An average 19.4 degree tilt of the anterior prostate was introduced due to ERC.
- The ability to align prostate MR images acquired with and without ERC was significantly improved when rigid ERC was employed (average percent overlap of ROI is 94.0 %).
- Hence, the alignment of prostate MRI/MRSI data acquired using an ERC with therapeutic planning MR images acquired without an ERC can be improved through the use of a rigid ERC.

Class solution for Inverse Planning

- The dose escalation on DIL is feasible for some patients under RTOG0321 dosimetric requirement in inverse planned HDR brachytherapy using MRI/MRSI information and class solution.
- Mostly the rectal dose prohibits the boost on DIL under RTOG0321 dosimetric requirement whenever the rectum is located closely to the prostate.

Reportable Outcomes

Summary of Reportable Outcomes

Task 1: To determine the need for alignment and to establish alignment methods for MRI/MRSI data to HDR brachytherapy treatment planning MRI and CT images. (Months 1-24).

a) To determine the need and accuracy of aligning MRI/MSRI data acquired with an ERC probe to images acquired without a probe (5 expandable versus15 rigid patient studies)

i. How misaligned a manually drawn ROI of the prostate is between the endorectal T2-weighted images and the T2-weighted images acquired without a probe, based on the following measures, computed for each image slice:

1. Translations in right/left (R/L), anterior/posterior (A/P), and superior/inferior (S/I): For the rigid ERC, the mean ± standard deviation (range) values are -2.31 ± 7.61 mm (-26.30 – 5.60 mm), -5.37 ± 3.77 mm (-10.60 – 4.20 mm), and 3.60 ± 3.62 mm (-3.00 – 9.00 mm) for R/L, A/P, and S/I direction, respectively.

2. Rotations in axial (Rot_{Axi}), sagittal (Rot_{Sag}), and coronal planes (Rot_{Cor}): The rotations of the prostate in coronal and axial planes (Rot_{Cor}, Rot_{Axi}) were visually negligible when we compared coronal and axial T2-weight MR image acquired with and without ERC. For the rotation of prostate in sagittal plane (Rot_{Sag}) due to rigid ERC coil, the mean ± standard deviation (range) values are -15.7 ± 14.5 degrees (-50.2 – 5.6 degrees).

3. Stretching/shrinking of right/left (R/L), anterior/posterior (A/P), and superior/inferior (S/I) axis were measured by the deformations ($D_{R/L}$, $D_{A/P}$, $D_{S/I}$) of prostate due to either expandable or rigid ERC: On average the expandable coil caused a significantly ($p < 0.05$) larger distortion of the prostate as compared to the rigid coil; compressing the prostate in the A/P direction by 4.7 ± 3.7 mm (mean ± standard deviation) versus 1.2 ± 2.2 mm (14.1% versus 3.9%), and widening the prostate in the R/L direction by 6.1 ± 2.8 mm versus 1.5 ± 3.1 mm (16.7% versus 4.2%).

4. Percent overlap of the ROI area (SI: Similarity Index): The stack of axial MR images acquired with coil was aligned with the stack of axial MR images without coil by rigid image registration (translation and rotation). The ability to align prostate images acquired with and without ERC was significantly ($p < 0.0001$) better for the rigid coil (SI = 0.941 ± 0.008, range from 0.925 to 0.952) than for the expandable coil (SI = 0.881 ± 0.04, range from 0.812 to 0.909).

ii. To determine if the proposed simple alignment method can produce less than 5% error for each measure listed in (i). The method is based on visually aligning manually drawn ROIs of the prostate acquired with and without a probe while incorporating translations, rotations and stretching and shrinking each axis on each slice: A 94% Average overlap of prostate contours was obtained using rigid ERC. Further investigation is needed for the alignment of non-endorectal MR images from coil-in MRI/MRSI exam to planning CT or MRI.

iii. To determine the tolerances of the alignment procedure for the measures listed in (i).

We will perform this study in 2005.

Task 2:   To elaborate class solutions (a set of optimization constraints) appropriate for DIL boosts of the order of 150% of the prescribed dose and protection for the penile bulb and the neuro-vascular bundle valid for 90% of the cases.

We obtained a class solution for the boost of DIL defined by MRI/MRSI and the maximum achievable boost level under RTOG0321 dosimetric requirement using 10 HDR brachytherapy patients.

a) To determine the parameters of the dose constraints for the protection of the penile bulb.
We will include the penile bulb for the class solution in the future.

b) To determine the ability of IPSA to limit the dose delivered to the neuro-vascular bundles while keeping an adequate coverage of the prostate. The first objective is to limit the dose to the bundles to 90%. Investigation will be required to determine if a lower value can be reached.

We will include the neuro-vascular bundles for the class solution as soon as MRI-based HDR brachytherapy patients are enrolled.

c) To determine the parameters of the class solution that will fulfill the DIL boost and simultaneously protect the additional organs at risk, bulb and neuro-vascular bundles.

i. To determine if the class solution can include all DIL locations within the prostate. Although most DIL are located in the peripheral zone of the prostate, a more central DIL might require heavier weighting on the urethra protection.

Task 3:   To perform feasibility and short-term measures of improved effectiveness and decreased side effects of performing the proposed treatment planning protocol in a small cohort of patients. (Months 18-36).

Task 3 will begin when we have approval for patient enrollment.

Details of Reportable Outcomes

Task 1: To determine the need for alignment and to establish alignment methods for MRI/MRSI data to HDR brachytherapy treatment planning MRI and CT images. (Months 1-24).

a) To determine the need and accuracy of aligning MRI/MSRI data acquired with an endorectal probe to images acquired without a probe (5 expandable versus15 rigid patient studies)

iv. How misaligned a manually drawn ROI of the prostate is between the endorectal T2-weighted images and the T2-weighted images acquired without a
probe, based on the following measures, computed for each image slice:

1. Translations in right/left (R/L), anterior/posterior (A/P), and superior/inferior (S/I).

For the rigid endorectal coil, the mean ± standard deviation (range) values are -2.31 ± 7.61 mm (-26.30 – 5.60 mm), -5.37 ± 3.77 mm (-10.60 – 4.20 mm), and 3.60 ± 3.62 mm (-3.00 – 9.00 mm) for R/L, A/P, and S/I direction, respectively. The following table summarized all the amount of translation due to either expandable or rigid endorectal coil in the unit of mm.

	Direction	Mean	SD.	Min.	Max.	Median
15 Rigid cases	S/I	3.60	3.62	-3.00	9.00	3.00
	R/L	-2.31	7.61	-26.30	5.60	-1.70
	A/P	-5.37	3.77	-10.60	4.20	-5.40
5 Expandable cases	S/I	5.40	6.50	0.00	15.00	3.00
	R/L	0.54	1.13	-0.80	1.90	0.20
	A/P	-9.86	2.67	-13.30	-6.50	-9.10
Total 20 cases	S/I	4.05	4.38	-3.00	15.00	3.00
	R/L	-1.60	6.67	-26.30	5.60	-0.50
	A/P	-6.50	3.99	-13.30	4.20	-6.45

Positive direction is left, posterior and superior direction.
SD: Standard Deviation, Min: Minimum, Max: Maximum

2. Rotations in axial (Rot_{Axi}), sagittal (Rot_{Sag}), and coronal planes (Rot_{Cor}).

The rotations of the prostate in coronal and axial planes (Rot_{Cor}, Rot_{Axi}) were visually negligible when we compared coronal and axial T2-weight MR image acquired with and without ERC. For the rotation of prostate in sagittal plane (Rot_{Sag}) due to rigid endorectal coil, the mean ± standard deviation (range) values are -15.7 ± 14.5 degrees (-50.2 – 5.6 degrees). The following table summarized all rotation angles due to either expandable or rigid endorectal coil in the unit of degree.

	Mean	SD.	Min.	Max.	Median
15 Rigid cases	-15.7	14.5	-50.2	5.6	-16.0
5 Expandable cases	-3.3	17.3	-27.5	18.0	-2.3
Total 20 cases	-12.6	15.8	-50.2	18.0	-13.0

Positive direction is counterclockwise
SD: Standard Deviation, Min: Minimum, Max: Maximum

3. Stretching/shrinking of right/left (R/L), anterior/posterior (A/P), and superior/inferior (S/I) axis were measured by the deformations ($D_{R/L}$, $D_{A/P}$, $D_{S/I}$) of prostate due to either expandable or rigid endorectal coil.

Figure 1 graphically summarizes the A/P (a) and R/L (b) distortions for the rigid (squares) and expandable (circles) ERCs at the base, midgland and apex of the prostate. On average the expandable coil caused a significantly ($p < 0.05$) larger distortion of the prostate as compared to the rigid coil; compressing the prostate in the A/P direction by 4.7 ± 3.7 mm (mean ± standard deviation) versus 1.2 ± 2.2 mm (14.1% versus 3.9%), and widening the prostate in the R/L direction by 6.1 ± 2.8 mm versus 1.5 ± 3.1 mm (16.7% versus 4.2%). Additionally, the expandable coil consistently caused larger distortions along the S/I length of the prostate (base, midgland and apex of gland) as compared to the rigid coil, with the distortions being significantly larger ($P < 0.05$) at all locations except

for the A/P dimension at the base and midgland due to the large variability of theses measurements (Fig. 1(a)). There was no significant difference in the degree of deformation with location (apex, midgland and base) for either ERC. The difference in the S/I length of the prostate measured between images acquired with and without either ERC was always less than the thickness of an axial MR image (3 mm).
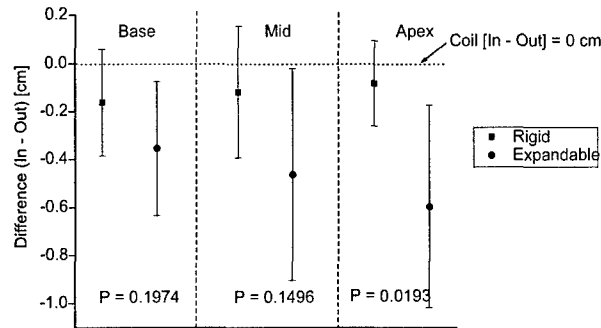

Figure 1(a)
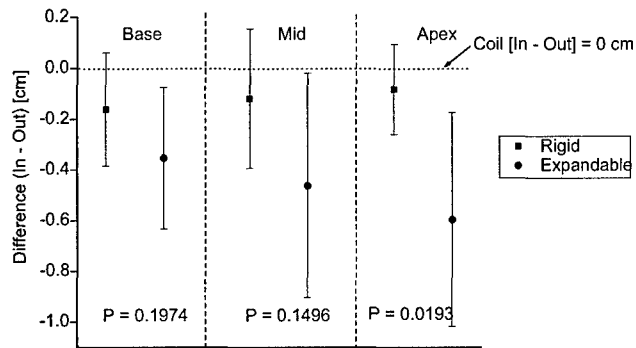
Figure 1(b)

4. Percent overlap of the ROI area.

The stack of axial MR images acquired with coil was aligned with the stack of axial MR images without coil by rigid image registration (translation and rotation). Figure 2 graphically demonstrates the improvement in the similarity index (Percent overlap of the prostate contours) attained using the rigid coil. Quantitatively, the ability to align prostate images acquired with and without ERC was significantly ($p < 0.0001$) better for the rigid coil (SI = 0.941 ± 0.008, range from 0.925 to 0.952) than for the expandable coil (SI = 0.881 ± 0.04, range from 0.812 to 0.909).


10
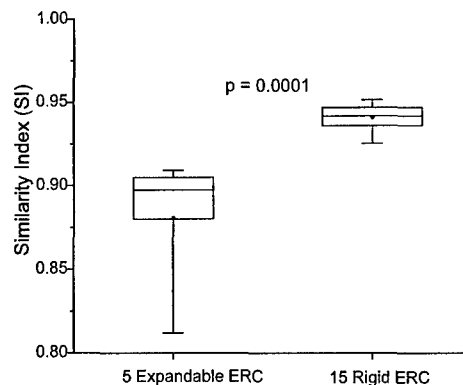
Figure 2

v. To determine if the proposed simple alignment method can produce less than 5% error for each measure listed in (i). The method is based on visually aligning manually drawn ROIs of the prostate acquired with and without a probe while incorporating translations, rotations and stretching and shrinking each axis on each slice.

A 94% Average overlap of prostate contours was obtained using rigid endorectal coil. Further investigation is needed for the alignment of non-endorectal MR images from coil-in MRI/MRSI exam to planning CT or MRI.

vi. To determine the tolerances of the alignment procedure for the measures listed in (i).

We will perform this study in 2005.

Task 2: To elaborate class solutions (a set of optimization constraints) appropriate for DIL boosts of the order of 150% of the prescribed dose and protection for the penile bulb and the neuro-vascular bundle valid for 90% of the cases.

We obtained a class solution for the boost of DIL defined by MRI/MRSI and the maximum achievable boost level under RTOG0321 dosimetric requirement using 10 HDR brachytherapy patients.

For 10 patients, DILs were manually contoured on HDR planning CT/MR images based on combined MRI/MRSI. A prostate was divided into 3 sectors in the cranio-caudal direction of the prostate (apex, mid and base of prosatate) on planning CT or MRI. A lesion containing at least 3 contiguous MRSI validated cancer voxels was called a DIL. The each voxel size of MRSI data is either 0.17 cc (for 5 patients) or 0.086 (for 5 patients). The mean ± standard deviation (range) values are 36.9 ± 5.1 cc (31.6 – 45.7 cc) for target volume and 13.5 ± 7.7% (3.7 – 31.3%) for the percentage of DIL volume over the target volume. The class solution of dose constraints, acceptable dose range and penalty values, were obtained from our previous clinical experience on inverse planning technique (IPSA) as following table.

Volume		Weight for D_{min}	D_{Min} (%)	D_{Max} (%)	Weight for D_{max}
PROSTATE Target	ON	100	100	150	100
	IN	100	100	150	30
URETHRA Organ at risk	ON	100	100	120	30
	IN	100	100	120	30
BLADDER Organ at risk	ON	-	-	50	30
	IN	-	-	-	-
RECTUM Organ at risk	ON	-	-	50	30
	IN	-	-	-	-

For each patient, six plans (one without-boost and 5 different levels of dose escalation to the DILs requesting a minimum of 110, 120, 130, 140 and 150% of the prescribed dose,

respectively) were generated using IPSA. The following table shows the class solution for 5 different boost levels of DIL.

Volume		Weight for D_{min}	D_{Min} (%)	D_{Max} (%)	Weight for D_{max}
DIL (110%) Target	ON	100	110	150	0
	IN	100	110	150	30
DIL (120%) Target	ON	100	120	150	0
	IN	100	120	150	30
DIL (130%) Target	ON	100	130	150	0
	IN	100	130	150	30
DIL (140%) Target	ON	100	140	150	0
	IN	100	140	150	30
DIL (150%) Target	ON	100	150	150	0
	IN	100	150	150	30

The dosimetric requirement of RTOG0321 protocol is V100 > 90% for target coverage, V75 < 1 cc for bladder and rectum, and V125 < 1 cc for urethra. For 5 different plans, the dosimetric indices were computed and compared with the dosimetric requirement.

Plans without boost satisfied all RTOG0321 requirements with average dose coverage of 92.1% to target (range from 90.6 to 93.8%). Four (B, C, D, and J) out of 10 patients prohibited any boost whereas a certain level of boost to the DILs was feasible for the rest of patients, minimum dose of 110% for patient E, 120% for patient H and I, 140% for patient A and F, and 150% for patient G, respectively. For each patient, the summary of dosimetric indices of without-DIL boost plan and maximum acceptable boost level plan (if available) are shown in the following table.

Patient	case	Target V100[%]	Bladder V75[cc]	Rectum V75[cc]	Urethra V125[cc]	DIL V120[%]	V150[%]
A	without	90.64	0.89	0.07	0.03	88.33	54.19
	140	92.71	0.94	0.85	0.27	93.02	53.03
B	without	93.46	0.53	0.51	0.11	71.67	29.67
C	without	91.85	0.98	0.29	0.00	95.29	42.07
D	without	90.73	0.00	0.91	0.17	81.52	40.04
E	without	91.97	0.64	0.24	0.02	53.22	29.49
	110	91.93	0.73	0.88	0.01	58.98	19.41
F	without	92.11	0.02	0.18	0.01	90.86	34.32
	140	92.00	0.02	0.91	0.00	97.26	62.70
G	without	93.78	0.03	0.61	0.00	99.74	63.01
	150	94.75	0.03	0.94	0.03	100.00	85.13
H	without	92.37	0.34	0.06	0.00	71.72	23.10

	120	94.01	0.41	0.94	0.12	77.24	34.16
I	without	92.85	0.03	0.21	0.08	79.53	38.86
	120	94.65	0.06	0.92	0.24	87.16	31.79
J	without	90.89	0.01	0.91	0.06	77.69	37.94

The violation of RTOG0321 protocol is rectal dose for 9 patients and bladder dose for patient C. The average benefit from maximum achievable boost for 6 patients is 1.1% increase of target coverage and 5% increase of V120 dose to DILs compared with a plan without boost.

d) To determine the parameters of the dose constraints for the protection of the penile bulb.
   We will include the penile bulb for the class solution in the future.

e) To determine the ability of IPSA to limit the dose delivered to the neuro-vascular bundles while keeping an adequate coverage of the prostate. The first objective is to limit the dose to the bundles to 90%. Investigation will be required to determine if a lower value can be reached.

   We will include the neuro-vascular bundles for the class solution as soon as MRI-based HDR brachytherapy patients are enrolled.

f) To determine the parameters of the class solution that will fulfill the DIL boost and simultaneously protect the additional organs at risk, bulb and neuro-vascular bundles.

   ii. To determine if the class solution can include all DIL locations within the prostate. Although most DIL are located in the peripheral zone of the prostate, a more central DIL might require heavier weighting on the urethra protection.

Task 3:   To perform feasibility and short-term measures of improved effectiveness and decreased side effects of performing the proposed treatment planning protocol in a small cohort of patients. (Months 18-36).

Task 3 will begin when we have approval for patient enrollment.

LIST OF ACRONYMS

CHR:	Committee on Human Research
CT:	Computed Tomography
MRI:	Magnetic Resonance Imaging
MRSI:	Magnetic Resonance Spectroscopic Imaging
DIL:	Dominant Intraprostatic Lesion
S/I:	Superior-Inferior
R/L:	Right-Left
A/P:	Antero-Posterior
DOD:	Department of Defense
ERC:	Endo Rectal Coil
GU:	Genito-Urinary Committee
HDR:	High Dose Rate
IPSA:	Inverse Planning with Simulated Annealing
MRI:	Magnetic Resonance Imaging
MRSI:	Magnetic Resonance Spectroscopy Imaging
PRC:	Protocol Review Committee
ROI:	Region of Interest
RTOG:	Radiation Therapy Oncology Group
SI:	Similarity Index
UCSF:	University of California, San Francisco
Vn[%]:	Percentage of Volume Receiving n% of the Prescribed Dose
Vn[cc]:	Volume in Cubic Centimeter Receiving n% of the Prescribed Dose

Appendices

## A   UCSF P.R.C. Committee approval letter

UCSF Comprehensive Cancer Center
Protocol Review Committee
Box 1297
Phone: 353-9512
Fax: 353-9738

July 12, 2004

Dear Dr. Pouliot:

Your protocol *CC #04554: Phase I Study of Targeting Dominant Intraprostatic Lesion Using Functional Imaging with MR Spectroscopy and High Dose Rate Brachytherapy* (dated June 6, 2004) has been approved as scientifically valid and logistically feasible by the UCSF Comprehensive Cancer Center Protocol Review Committee (PRC). The approval date is **July 7, 2004**. You may now submit this letter and your protocol to the UCSF Committee on Human Research (CHR). You should then submit one copy of your CHR Approval letter to the Protocol Office. The status of this protocol will be reviewed annually until it is closed to accrual.

Sincerely,

Judith Luce, MD /rr
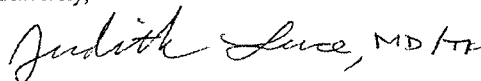
Judith A. Luce, M.D.
Chair, Protocol Review Committee

Form Revised 11/05/03

15

B   **UCSF C.H.R. Committee approval letter**

COMMITTEE ON HUMAN RESEARCH
OFFICE OF RESEARCH, Box 0962
UNIVERSITY OF CALIFORNIA, SAN FRANCISCO
www.research.ucsf.edu/chr/Apply/chrApprovalCond.asp
chr@ucsf.edu
(415) 476-1814

CHR APPROVAL LETTER

TO: Jean Pouliot, Ph.D.   I-Chow Joe Hsu, M.D.
       Box 1708   Box 1708,

RE: Phase I Study of Functional Targeting of Dominant Intraprostatic Lesion Using MR Spectroscopy for Prostate High Dose Rate Brachytherapy Boost

The Committee on Human Research (CHR) has reviewed and approved this application to involve humans as research subjects. This included a review of all documents attached to the original copy of this letter.

     Specifically, the review included but was not limited to the following documents:
     Consent Form, dated 12/17/04

The CHR is the Institutional Review Board (IRB) for UCSF and its affiliates. UCSF holds Office of Human Research Protections Federalwide Assurance number FWA00000068. See the CHR website for a list of other applicable FWA's.

APPROVAL NUMBER: H11386-24294-01. This number is a UCSF CHR number and should be used on all correspondence, consent forms and patient charts as appropriate.

APPROVAL DATE: December 17, 2004   **EXPIRATION DATE:** December 17, 2005   **Full Committee Review**

GENERAL CONDITIONS OF APPROVAL: Please refer to www.research.ucsf.edu/chr/Apply/chrApprovalCond.asp for a description of the general conditions of CHR approval. In particular, the study must be renewed by the expiration date if work is to continue. Also, prior CHR approval is required before implementing any changes in the consent documents or any changes in the protocol unless those changes are required urgently for the safety of the subjects.

HIPAA "Privacy Rule" (45CFR164): This study requires individual consent/authorization for use and/or disclosure of Protected Health Information (PHI).

Sincerely,

Victor I. Reus, M.D.
Chair, Committee on Human Research

cc: Alan Taniguchi, Box 1708

C   Publications

1- Jean Pouliot, Yongbok Kim, Etienne Lessard, I-Chow Hsu, Daniel B. Vigneron and John Kurhanewicz, Inverse Planning For HDR Prostate Brachytherapy Used To Boost Dominant Intraprostatic Lesions Defined By Magnetic Resonance Spectroscopy Imaging, *Int. J. Radiation Oncology Biol. Phys.*, Vol. 59, No. 4, pp. 1196–1207, 2004.

2- Yongbok Kim, Susan Moyher Noworolski, Jean Pouliot, I-Chow J. Hsu, Daniel B. Vigneron, and John Kurhanewicz, Expandable and rigid endorectal coils for prostate MRI: Impact on prostate distortion and image registration, *submitted for publication to Medical Physics*, January 2005.

-1-

INVERSE PLANNING FOR HDR PROSTATE BRACHYTHERAPY USED TO BOOST DOMINANT INTRA-PROSTATIC LESION DEFINED BY MAGNETIC-RESONANCE SPECTROSCOPY IMAGING

JEAN POULIOT, PH.D.,* YONGBOK KIM, M.SC.,* ETIENNE LESSARD, M.SC.,* I-CHOW HSU, M.D.*

DANIEL B. VIGNERON,† PH.D., AND JOHN KURHANEWICZ,† PH.D.

Departments of *Radiation Oncology and †Radiology, University of California San Francisco,

San Francisco, Ca.

Corresponding author: Jean Pouliot, Ph.D., Department of Radiation Oncology,

University of California, 1600 Divisadero St., Suite H1031, San Francisco, Ca-94143-1708

E-mail: pouliot@radonc17.ucsf.edu

Fax: 415 353-9883

URL : www.ucsf.edu/jpouliot

Running title : MRI/MRSI-based Inverse planning for HDR Brachytherapy

Abstract

Purpose: To dose escalate selected regions inside the prostate without compromising the dose coverage of the prostate and the protection to the urethra, rectum and bladder for prostate cancer patients treated with HDR brachytherapy.

Methods & Materials: Magnetic resonance imaging combined with magnetic resonance spectroscopy imaging was used to differentiate between normal and malignant prostate and define cancer-validated dominant intra-prostatic lesions (DIL) on 10 patients. The DIL were then contoured on the planning scans (CT or MRI based, 5 patients each) and our inverse planning dose optimization algorithm (called IPSA) was used to generate dose distributions for three different boost levels. Dose volume histograms of the target and each organ at risk were compared with optimized plans without DIL boost.

Results: Combined MRI/MRSI identified two DILs in 8/10 of the ten patients studied, and a single DIL in the remaining two patients. The average prostate dose coverage V100 was 97% (σ=1.0%). When the minimum DIL dose requested was 120% of the prescribed dose, the average DIL V120 was 97.1% (σ=1.8%). For a boost value of 150%, the average V150 ranged from 77.8% to 86.1% depending on the upper limit of the dose constraints. The bladder V50 increased by 1%, independently of the boost levels. The absolute increases in V50 for the rectum varied from 1 to 3% depending on the boost level. The urethra V120 were increased by 13.4% and 32.5 % for the lowest and highest boost levels, respectively.

Conclusion: The DIL dose can be escalated to a minimum of 120%, while simultaneously treating the entire prostate without increasing the dose to surrounding normal tissues. Higher boost levels between 150% and 170% are feasible, but with slightly larger doses delivered to the rectum and urethra.

Key words: Magnetic resonance spectroscopy imaging MRSI, Prostate cancer, High Dose Rate Brachytherapy, HDR, Inverse planning dose optimization, Dominant intra-prostatic lesion, Dose escalation.

INTRODUCTION

The advent of functional imaging modalities such as Positron-Emission Tomography (PET) or combined MRI/MR-spectroscopy imaging (MRSI) provides new tools for better cancer-validated tumor targeting in radiation therapy. Magnetic Resonance Spectroscopic Imaging (MRSI) provides a non-invasive method of detecting small molecular markers (e.g. the metabolites choline, citrate and polyamines) within the cytosol and extracellular spaces of the prostate and is performed in conjunction with high-resolution anatomic imaging (MRI). Combined MRI/MRSI can be used to improve the radiation dose distribution in two important ways. First, high spatial resolution MRI can provide improved definition of the prostate, its complex zonal anatomy, and important surrounding structures. Secondly, a combination of MRI/MRSI and biopsies can be used to define the distribution of dominant regions of cancer within the prostate. Specifically, it has been demonstrated that the high specificity of MRSI to metabolically identify cancer can be used to improve the ability of MRI to identify the location and extent of cancer within the prostate [1]. A study of 53 biopsy proven prostate cancer patients prior to radical prostatectomy and step-section pathologic examination demonstrated a significant improvement in cancer localization to a prostatic sextant (left and right – base, mid-gland, and apex) using combined MRI/MRSI versus MRI alone [2]. A combined positive result from both MRI and MRSI indicated the presence of tumor with high specificity (91%) while high sensitivity (95%) was attained when either test alone indicated the presence of cancer. In another study it was found that the addition of a positive sextant biopsy finding to concordant MRI/3D MRS findings further increased the specificity (98%) of cancer localization to a prostatic sextant, whereas high sensitivity (94%) was again obtained when any of the tests alone were positive for cancer [3]

This information can be used to dose escalate only the cancer-validated area within the prostate, defined as the Dominant Intraprostatic Lesion (DIL). Picket et al., [4] have demonstrated the feasibility of using MR-spectroscopy to dose escalate dominant intra-prostatic lesion with external beam. By combining IMRT and MRSI, Xia et al., [5] were able to treat the DIL to 90 Gy, while simultaneously treating the prostate to > 70 Gy without increasing the dose to surrounding normal tissues. The combination of an optimization planning algorithm, MR-spectroscopy (MRSI) and tumor control probability (TCP) has proven to be a safe approach to escalate dose and possibly improve outcome of patients treated with permanent implanted seeds [6]. In their study, Zaider et al demonstrated that a minimum dose of 120% of the 144 Gy prescription could be delivered to the DIL using ^{125}I seeds. Yet, these important pieces of information (MRS and TCP-NTCP) have not been taken into account in treatment planning of high dose rate (HDR) brachytherapy.

Recently, Hsu et al [7] compared the dose and volume of bladder and rectum treated using HDR brachytherapy versus conformal external beam radiotherapy boost and found that the volume of bladder and rectum receiving high dose was significantly less — about 95 % — with implant boost. With this kind of protection to the adjacent organs at risk, they concluded that HDR brachytherapy has a potential for dose escalation beyond external radiotherapy limits. Theoretical studies have suggested this can significantly improve tumor control probability. Furthermore, the fact that HDR brachytherapy uses an afterloading unit to move a single radioactive seed (^{192}Ir) along many temporarily implanted catheters makes it possible to generate a wide variety of dose distributions from a given implant simply by adjusting the length of time (dwell time) that the source dwells at any location within a catheter (dwell position). This flexibility allows the full benefit of the 3-dimensional planning system based on CT or MRI.

The purpose of this study is to demonstrate the feasibility of DIL dose escalation for prostate HDR Brachytherapy. We have applied our in-house developed inverse planning optimization algorithm to increase the dose delivered to the dominant intra-prostatic lesions defined by MRI/MRSI and evaluated the impact on the dose coverage of the prostate and the protection to the urethra, rectum and bladder. Different values of DIL boosts were computed to establish to what extent the DIL dose can be increased without affecting the dose delivered to the organs at risk while maintaining the prostate dose coverage.

METHODS AND MATERIAL

The study was performed on 10 patients treated for prostate cancer with HDR brachytherapy. The locations of the DIL, as determined from the combined MRI/MRSI scans, were manually contoured on the planning scans. For this study, dose planning was based on CT scans for 5 patients and on MRI for another 5. For each patient, our in-house inverse planning routine was used to optimize the dose distribution and dose escalate three levels of DIL boosts to be compared with the reference plan with no boost. Dose Volume Histograms (DVH) of the target and each organ at risk were computed and the results compared with optimized plans without DIL boost.

MRSI/MRI Acquisition

The details of the MRI/MRSI techniques have been previously described [8,9]. In brief, patients received Internal Review Board (IRB) approved-consent and MRI/MRSI scans were obtained on a 1.5 Tesla GE system to determine the location of the cancer-validated dominant intraprostatic lesions (Signa; GE Medical Systems, Milwaukee, WI) [9]. Patients were scanned in the supine position using the body coil for excitation and a pelvic phased array coil (GE Medical Systems, Milwalkee, WI) in combination with a commercially available balloon-covered expandable endorectal coil (Medrad, Pittsburgh, PA) for signal reception. Axial spin-echo T1 weighted images were obtained from the aortic bifurcation to the symphysis pubis, using the following parameters: TR/TE = 700/8 msec, slice thickness = 5 mm, interslice gap = 1 mm, field of view = 24 cm, matrix 256 x 192, frequency direction transverse, and 1 excitation. Thin-section high spatial resolution axial and coronal T2 weighted fast spin-echo images of the prostate and seminal vesicles were obtained using the following parameters: TR/effective TE 6000/96 msec, echo train length = 16, slice thickness = 3 mm, interslice gap = 0 mm, field of view = 14 cm, matrix 256 x 192, frequency direction anteroposterior (to prevent obscuration of the prostate by endorectal coil motion artifact), and 3 excitations. All MR images were post-processed to compensate for the reception profile of the endorectal and pelvic phased array coils [1].

After review of the axial T2 weighted images, a spectroscopic imaging (MRSI) volume was selected to maximize coverage of the prostate, while minimizing the inclusion of periprostatic fat and rectal air. This was achieved using a water and lipid suppressed double-spin echo PRESS (Point-Resolved Spectroscopy) sequence, in which both 180° pulses were replaced with dualband phase compensating spectral/spatial pulses designed for robust spectroscopic volume selection and water and lipid suppression [10]. The ability to include all of the prostate in the spectroscopic volume while minimizing spectral contamination from outside the gland was improved by applying very selective suppression (VSS) pulses to better define the sides of the PRESS volume and conform the rectangular volume to fit the shape of the prostate [11]. Subsequent to volume selection, 16 x 8 x 8 phase encoding was applied to produce spectral arrays having spectroscopic voxels with a nominal spatial resolution of 0.3 cm^3, TR/TE = 1000/130 ms, and 17 minute acquisition time. The total examination time was 1 hour, including, coil placement and patient positioning.

Spectroscopic data were processed using a combination of in-house and IDL (Research Systems, Inc., Boulder, CO) software tools. Spectra were evaluated after automatic phasing, frequency alignment and baseline correction. Metabolite peak areas were obtained by numerical integration over regions corresponding to choline, creatine, and citrate, and the loss of polyamines in cancer was qualitatively assessed by the associated improved resolution of the choline and creatine resonances. Spectra were inspected and compared with the corresponding axial T2-weighted image and were considered useable if less than 25% of the voxel was in the central gland, the voxel did not contain urethral or ejaculatory ducts tissue, and the spectra were not contaminated by insufficiently suppressed water or lipid. Abnormal spectra within the central gland were only called if the abnormality extended from the peripheral zone or very elevated choline (Choline/Creatine > 2) was observed. The elimination of spectral contamination from outside the PRESS volume allowed the interpretation of peripheral zone voxels that extended outside of the PRESS volume as there was sufficient signal-to-noise. All useable spectral voxels were scored using a standardized

five-point scale recently developed for the interpretation of peripheral zone metabolism [12]. Based on changes in choline, citrate and polyamines, a score from 1 to 5, was assigned to each spectroscopic voxel. A score of 1 was considered to be definitely benign, 2 likely benign, 3 equivocal, 4 likely abnormal, and 5 definitely abnormal. Because MRSI and MRI are acquired within the same exam, the data sets are already in alignment and can be directly overlaid (Figures 1A and B). However, the endorectal coil necessary for the acquisition of the high resolution MRSI data distorts the shape of the prostate. The acquisition of images with and without the endorectal coil within the same exam improved the translation of the MRSI data to the non-distorted images for manual merging with the planning CT or MRI scans. The DILs were identified as regions of 3 or more adjacent abnormal spectroscopic voxels (scores of 4 and/or 5) with a corresponding anatomic abnormality (decreased signal intensity on T2-weighted images).

The patient population is described in Table I. All patients had biopsy proven prostate carcinoma. The prostate volumes range from 30 to 45 cc. The DIL volumes ranged from 0.4 cc to 6.0 cc, representing 5 to 18 % of the prostate volumes. Eight of the ten patients showed two distinct DIL volumes (or foci). In all cases, the DIL were located in the peripheral zone of the gland.

Using MRSI/MRI information to define DIL on Planning Scans (CT or MRI)
A volume study (CT or MRI planning scan) with the catheters in place was performed for dose planning purpose immediately after catheter insertion. The transversal planning CT (or MRI) and MRSI/MRI slices were aligned manually to match the corresponding anatomical structures. On each slice, the observer reproduced the DIL contours based on MRI and MRSI. The transversal alignment was based on mutual anatomical features and was, for the most part, straightforward. Few simple rules were followed to insure consistency throughout the process. In particular, the distances from the DIL to the urethra (laterally) and the rectum were used to position the DIL on each slice. As a final consistency check, the volume of the DIL contoured on the planning scan was compared to its volume on the MRSI scan. For this study, the distortion of the prostate was only addressed visually. For example, the urethra appears more posterior on the MRSI than on the planning scans due to the compression of the endorectal probe. The uncertainty is limited by the fact that MRSI was used to determine the DIL locations, representing only a small volume, limited to the peripheral zone of the prostate. The longitudinal alignment was complicated by the fact that CT slice thicknesses were 3 mm while MRI/MRSI reconstructed slices were 3.5 mm. For CT-based dose planed, the MRI/MRSI defined DIL were contoured to the nearest cranio-caudal CT slice coordinates. This resulted in a precision of 1.5 mm in the longitudinal definition of the DIL. No restrictions on the minimum distance between the DIL and the rectum or urethra were imposed in delineating the DIL contours. Therefore, on several occasions, the DIL was very close to the rectum.

Inverse Planning Dose Optimization
The dose planning tool developed and routinely used clinically at our institution (IPSA - Inverse planning – simulated annealing) [13-16] was used to perform the dose distribution optimization in this study. The program combines two parts: 1) a user-to-computer translator that gathers the anatomical dose constraints of the physician, and 2) an optimization engine that finds the best solution that fulfills the dose constraints. Clinical Target Volumes (CTV) and Organs at Risk (OAR) are contoured on each slice of the scan used for CT or MRI based planning. Active dwell source positions are automatically selected from all possible dwell positions based on CTV and OAR and dwell times are automatically optimized.

The standard dose constraints include dose coverage for the prostate with an acceptable dose range within the prostate to limit heterogeneity in the dose distribution, protection against hot spots to the urethra, minimization of the dose delivered to the bladder, bulb and rectum. It was previously shown that the inverse planning approach IPSA provides superior HDR plans from a dosimetric point of view than do regular forward planning approaches. This is particular the case when, in addition to dose coverage, 3D anatomical

dose conformity (sparing of normal tissue), uniformity and protection to organs at risk are considered [13,15,16].

In the present work, in addition to the dose constraints imposed on the prostate, urethra, bladder, bulb, rectum and normal tissues, three different boost levels were defined for the DIL. The Table II presents how the acceptable dose range is specified. For each volume of interest, two sets of values, used to constrain the dose on the contours (ON) and inside the volume (IN), must be provided. A minimum dose (D_{min}) and a maximum dose (D_{max}) define the acceptable dose range. When the dose to any given dose point is within this range, the optimization does not attempt to modify it. Penalties are applied when the dose is out of this range. Penalty or weight factors are associated with minimum and maximum doses outside the acceptable dose range, respectively [13-15].

The 100% isodose is specified as the prescribed dose. Therefore, in Table II, a minimum dose of 100% is required for the prostate gland, both on the contour (ON) and inside the gland (IN). The weight given to this is maximum or 100. The maximum dose tolerated represents 150% of the prescribed dose. Inside the volume, more small hot spots must be tolerated very close to each source. Therefore the weight for high dose inside is reduced (30). For the urethra, the minimum prescribed dose is required, but the maximum dose must be limited to 120%. The dose range in Table II is therefore 100 to 120% on the contours and inside the volume.

IPSA automatically turns off all dwell source positions inside an OAR. It is therefore not necessary to specify an acceptable dose range inside an organ at risk, but only on its surface. The concept of prescribing at a given point no longer applies for inverse planning; the prescription is global. One of the advantages of this approach is that the burden on the user does not increase with the number of targets or organs at risk. Additional volumes of interest are simply added in the dose constraints by introducing a new volume and specifying the parameters for ON and IN.

IPSA was used to generate four optimized dose distributions for each patient; one without DIL boost and one for each DIL boost level. For boost level 1 (B1), dose constraints were defined to bring the dose to the DIL to fall within the range of 120 and 150% of the prescribed dose. A second boost level, B2 required both a minimum and maximum dose of 150%. Finally, a third boost B3, was designed to push the dose above 150% of the prescribed dose, but less than 170%. The corresponding DIL constraints for different boost levels (B1, B2 and B3) are presented in Table II. For patients with 2 DIL, the same set of dose constraints was applied to both DIL. For a given boost level, the set of the same dose constraints represents a class solution and was used to govern the dose optimization of all patients. Here, we have exploited the main feature of IPSA where several targets and organs at risk can be simultaneously taking into account, including the case of one (or several) target within a target (DIL boost).

The V100 and V150 were extracted from the DVH to assess target dose coverage and homogeneity for each DIL boost level and without boost. For the DIL, V100, V120 and V150 were recorded. Dose delivered to bladder and rectum was verified using V50 and V80. V100 and V120 were recorded for the urethra.

RESULTS
Figure 1 shows a representative reception-profile corrected T2 weighted FSE axial image taken from a volume data set of a patient who has two dominant intraprostatic lesions. The dominant intraprostatic lesions were identified by the presence of 3 or more contiguous spectroscopic voxels having scores higher than 3, and corresponding low signal intensity on T2 weighted imaging. As can be seen from the spectra scored as 4 or 5 (Fig. 1D), there was significantly decreased citrate and polyamines and increase choline relative to healthy spectra, scored as 1 and 2, or indeterminate spectra, scored as 3 (Figure 1C). In this study, combined MRI/MRSI identified two DILs in 8 of the ten patients studied, and a single DIL in the remaining two patients.

Isodose distributions for the reference plan and for the three different boost levels B1, B2 and B3 are presented on Figure 2 for the patient studied on Figure 1. The contours of anatomical structures (prostate (dashed line), urethra (hexagonal), rectum, and DIL (dotted line)) are shown here on the CT median slice. Three isodose levels are displayed, from outside in; 100, 150 and 200% of the prescribed dose. The dose coverage (V100) is similar for all boost levels. For this patient, one of the DILs is located close to the posterior limit of the prostate, resulting on the 100% isodose covering more rectum area as the boost level increases.

A set of DVHs for the target (Figure 3A), the two DIL included in the prostate (Figure 3, B and C) and for the organs at risk (Figure 4), bladder (A), rectum (B) and urethra (C) are presented for the same patient presented at Figures 1 and 2. Results from the other patients were very similar. Therefore, the specific results of this patient are typical of all the other patients analyzed. Each graph presents the DVH for 4 cases; reference plan (thin solid line), and three levels of boost, B1 (120 to 150%, dashed line), B2, (150 to 150%, dotted line) and B3 (150 to 170%, solid line). The first two cases (no boost and B1) are so similar that the curves are hardly distinguishable on the target DVH on Figure 3 A. DVHs for B2 and B3 are almost superimposed, either for target than organs at risk. The DVH curves for B2 and B3 are slightly above the reference plan or boost B1, either for the target (Figure 3 A) or the organs at risk (Figure 4 A,B and C). The main impact of DIL boost can be seen on the DIL DVHs on Figure 3 B and C.

In order to evaluate the global impact of the various boost levels on the dose delivered to the target and the organs at risk, the evolution of the dosimetrical indices (V50(%) for bladder and rectum and V120(%) for the urethra) of each individual patient for the reference plan, B1, B2 and B3 are presented on Figure 5 and 6. The absolute differences over all patients between the three boost levels (B1, B2 and B3) and the reference plan without boost are also presented in Table III. The small standard deviation values (numbers in parentheses in the Table) indicate the consistency among different patients.

For all boost levels, including the reference plans, the average target V100(%) (Figure 5 A, left) are above 96% (range 94 to 99%). The average V150(%) values of the prostate for all patients, were 38.1% for the reference plans and increased to 40.4%, 49.3% and 50.6% for the boost levels B1 to B3, respectively (Figure 5A, right). The increased V150 values for boosts B2 and B3 are simply due to the dose constraints imposing that the dose delivered to the DIL, included in the prostate DVH, be of at least 150% of the prescribed dose. It is interesting to note that the V150 shows very little increase between no boost and B1.

The DIL DVHs were analyzed to determine the degree of fulfillments of the dose constraints (Figure 5 B, left and right). For a boost level B1, the minimum dose requested was 120% of the prescribed dose and the average DIL V120 is 97.1% (standard deviation of 1.8%). For B2, the minimum boost value was 150% of the prescribed dose. The average V150 is 77.8% ($\sigma = 12\%$). Finally, for B3 the minimum dose value was as for B2 but the upper limit set to 170% of the prescribed dose. The V150 is 86.1% ($\sigma = 9.5$).

Figure 6 presents the results for the organs at risk. The V50s of the bladder (A) increase by an absolute value of about 1% for the various boost levels (0.97, 1.33 and 1.25 for B1, B2 and B3, respectively). The increases of V50 are probably clinically insignificant for the different boost levels compared to the reference plan. The absolute increases in V50 for the rectum is less than 1% for a B1 boost and about 3% for B2 and B3 boosts (Figure 6 B). However, the volume of the urethra receiving more than 120% of the prescribed dose is increased by 13.4% for a B1 boost and by 32.0 and 32.5 % for B2 and B3 boosts relatively to the reference plan, respectively (Figure 6 C). No attempt was made to minimize the dose increase to the urethra by imposing more weight on the protection of the urethra. Effectively, in order to perform an objective comparison, the same class solution was used among all plans with various boost levels as well as the reference plan.

DISCUSSION

In this cohort of patients, the different boost levels resulted in the urethra experiencing the largest increase. It should be noted that in spite of the maximum increase due to the B3 boost, the doses that would be delivered to the urethra were still below the doses that were planed and used clinically before the clinical introduction of the inverse planning tool [15]. The largest urethra dose increases were observed for the patients where the initial doses in the reference plan were the lowest. The optimization tool IPSA could therefore increase the dose to the urethra and still fulfill the new dose constraints including the DIL. For the patients with already a large V120%, little increases of the urethra doses were observed as the limits of the dose constraints were reached. Such a behavior would be very difficult to achieve with manual adjustments and only an anatomy based dose optimization tool such as the one used in this work could systematically refine the dose distribution to this extent.

In the future, MRI/MRSI scans could be performed with catheters already implanted. The catheters would provide additional landmarks that would facilitate the MRI to MRS image registration. Moreover, the MRI/MRSI scans could be used directly for dose planning. Before this can become possible however, the impact of the presence of the catheters as well as the trauma caused to the gland by their insertion on the spectroscopic responses of the MRS scans will need to be studied. In the present study, the transversal CT/MRI slices used for dose planning were aligned manually to match the corresponding anatomical structures. Then, the observer reproduced the DIL contours based on MRI and MRSI. Therefore, the distortion of the gland, due to the presence of the endorectal probe during the MRSI study, the swelling caused by the insertion of the catheters, or the presence of a Foley catheter in the urethra, was only accounted for visually. This is probably adequate on a limited number of patients and small DILs such as the cohort of this study. For routine clinical work however, one will need to establish alignment methods for MRI/MRSI data to HDR brachytherapy treatment planning MRI and CT images. This work is in progress.

In brachytherapy, a prostate optimized without boost would naturally show many dose areas above 120%. By requesting a B1 boost, the optimization has only to insure that the naturally occurring hot spots will fall where the DIL are located. The total dose delivered without boost and with a B1 boost is therefore the same; the dose is distributed differently. In fact, when comparing the total dwell time for the different boost levels, B1 was only 2% more than the reference plan. The total dwell times for B2 and B3 are 6% longer than the reference plan.

Although this paper addressed the feasibility to dose escalate a cancer-validated zone in the prostate, it could be argued that only the DIL plus a margin should receive the full prescribed dose, allowing to reduce the dose delivered to the rest of the prostate. This would result in a strong reduction of dose delivered to the surrounding tissues and organs at risk. However, better radiobiological data, perhaps gathered from functional imaging, will need to be obtained before dose reduction could be considered.

CONCLUSION

In this paper, we have demonstrated the feasibility of DIL dose escalation for prostate high dose rate Brachytherapy. We have exploited the high specificity of combined MRI/MRSI for detecting and localizing prostate cancer within the prostate to identify the dominant intraprostatic lesions. We have used our inverse planning dose optimization tool to increase the dose delivered to the DIL to the 120 to 150% range, while preserving the prostate coverage and keeping the dose delivered to the organs at risk to the same level compared to an inverse planned dose distribution without DIL boost. The B1 boost provided DIL dose levels to 120% with no increase of the dwell times. This is the nature of the inverse planning ability to move the hot spots where appropriate, in that case the DIL. This is inherently difficult to achieve with forward planning. Inverse planned DIL boosts of at least 120% can therefore be safely delivered. Larger boost values between 150% and 170% will have to be investigated before their clinical use can be considered.

REFERENCES

1. Kurhanewicz J., Vigneron D. and Nelson S.J., Three-Dimensional Magnetic Resonance Spectroscopic Imaging of Brain and Prostate Cancer, Neoplasia 2000;2 (1-2): 166-189.

2. Scheidler J, Hricak H, Vigneron DB, Yu KK, Sokolov DL, Huang LR, Zaloudek CJ, Nelson SJ, Carroll PR, Kurhanewicz J. Prostate cancer: localization with three-dimensional proton MR spectroscopic imaging--clinicopathologic study. Radiology1999; 213(2):473-80,.

3. Wefer AE, Hricak H, Vigneron DB, et al. Sextant localization of prostate cancer: comparison of sextant biopsy, magnetic resonance imaging and magnetic resonance spectroscopic imaging with step section histology [see comments]. J Urol 2000; 164:400-404.

4. Pickett B., Vigneault E., Kurhanewicz J., Verhey L. and Roach III M., Static Field Intensity Modulation to Treat a Dominant Intra-Prostatic Lesion to 90 Gy Compared to Seven Field 3-Dimensional Radiotherapy, Int. J. Radiation Oncology Biol. Phys. 1999: 43 (4):921-929.

5. Xia, P., Pickett B., Vigneault E., Verhey L. and Roach M. Forward or inversely planned segmental multileaf collimator IMRT and sequential tomotherapy to treat multiple dominant intraprostatic lesions of prostate cancer to 90 Gy. Int. J. radiation Oncology Biol. Phys. 2001; 51 (1): 244-254, 2001.

6. Zaider M., Zelefsky M.J., Lee E.K., Zakian K.L., Amols H.I., Dyke J., Cohen G., Hu Y.C., Endi A.K., Chui C.S. and Koutcher J., Treatment Planning for Prostate Implants Using Magnetic-Resonance Spectroscopy Imaging, Int. J. Radiation Oncology Biol. Phys. 2000; 47 (4):1085-1096.

7. Hsu I-C., Pickett B., Shinohara K., Krieg R. Roach III M. and Phillips T., Normal Tissue Dosimetric Comparison Between HDR Prostate Implant Boost and Conformal External Beam Radiotherapy Boost: Potential for Dose Escalation, Int. J. Radiation Oncology Biol. Phys.2000; 46 (4): 851-858.

8. Hricak H, White S, Vigneron D, et al. Carcinoma of the prostate gland: MR imaging with pelvic phased-array coils versus integrated endorectal--pelvic phased-array coils. Radiology 1994; 193:703-709.

9. Kurhanewicz J, Vigneron DB, Hricak H, Parivar F, Nelson SJ, Shinohara K and Carroll PR. Prostate cancer: metabolic response to cryosurgery as detected with 3D H-1 MR spectroscopic imaging. Radiology 1996; 200(2): 489-96.

10. Schricker AA, Pauly JM, Kurhanewicz J, Swanson MG, Vigneron DB. Dualband Spectral-Spatial RF Pulses for Prostate MR Spectroscopic Imaging. Magn. Reson in Med. 46: 1079-1087,

11. Tran TK, Vigneron DB, Sailasuta N, et al. Very selective suppression pulses for clinical MR spectroscopic imaging studies of brain and prostate cancer. Magn Reson Med 2000; 43:23-33.

12. Jung J.A., Coakley F.V., Qayyum A., Swanson, M.G., Vigneron D.B., Weinberg V., Jones K.D., Carroll P.R., Kurhanewicz J., "Endorectal MR spectroscopic imaging of the prostate: Investigation of a standardized evaluation system" Radiology 2003 , in press.

13. Lessard E. and Pouliot J., Inverse Planning Anatomy-based dose optimization for HDR-Brachytherapy of the prostate using fast simulated annealing algorithm and dedicated objective function, Med. Phys. 2001; 28 (5): 773-779.

14. Lessard, E., Hsu I-C. and Pouliot J., Inverse Planning For Interstitial Gynecological Template Brachytherapy: Truly Anatomy Based Planning, Int. J. Radiation Oncology Biol. Phys. 2002; 54 (5): 1243-1251.

15. Hsu I-C., Lessard E., Weinberg V., Pouliot J. Ph.D. Comparison of Inverse Planning Simulated Annealing and Geometrical Optimization for Prostate High Dose Rate Brachytherapy, Brachytherapy J. 2003. *in press*.

16. Lachance, B., B.-Nadeau, D., Lessard, E., Chrétien, M., Hsu, I.C., Pouliot, J., Beaulieu, L. and Vigneault E. Early Clinical Experience with anatomy-based inverse planning dose optimization for HDR boost of the prostate, Int. J. Radiation Oncology Biol. Phys. 2002; 54 (1): 86-100.

Figure and Table Captions

Figure 1. A) A representative reception-profile corrected T2 weighted FSE axial image taken from the midgland of a 63 year old patient with biopsy proven bilateral Gleason 4+3 cancer. The PRESS selected volume encompassing the prostate is overlaid as a bold white box and a portion of the 16x8x8 spectral array grid from one of 9 axial spectroscopic slices is overlaid on the axial T2 weighted image **(B)** with the corresponding axial 0.3 cm^3 proton spectral array **(C)**. The location of the spectral grid can be changed in post-processing to optimally align with regions of interest such as the peripheral zone. The DILs were identified as 3 or more adjacent voxels having scores greater than 3 as shown on a series of summary MRI/MRSI images (6 out of 9 images shown) **(D)**. Consistent with biopsy results two dominant intraprostatic images were identified, one in the left and one in the right lobe extending from the base to the apex.

Figure 2: Isodose distribution for the patient study presented on Figure 1 for the three boost levels B1, B2 and B3: The goals for the dose range in the DIL are for B1; 120% -150%, B2; 150%150% and B3; 150%-170%. The DIL are displayed as the light shaded areas. Only the areas with a score 4 (probably cancer) or 5 (definitively cancer) from Figure 1 were selected to define the DIL. The contours of anatomical structures (prostate (dashed line), urethra (hexagon), rectum, and DIL (dotted line)) are also shown here on the CT median slice. Three isodose levels are displayed, from outside to inside; 100, 150 and 200%.

Figure 3: Dose Volume Histograms of the prostate and of the DILs (in CC). The thin line represents the DVH for the reference plan (target only), and the other curves represent the three levels of boost, B1 (dashed line), B2 (dotted line) and B3 (solid line). The relative prescription dose was 100%.

Figure 4: Dose Volume Histograms of A) bladder (in CC), B) rectum (in CC), and C) urethra (in CC). The thin lines represent the DVH for the reference plan, and the other curves represent the three levels of boost, B1 (dashed line), B2 (dotted line) and B3 (solid line).

Figure 5: Values of A) V100(cc) (left) and V150(%) (right) of the prostate, and B) V120 (%) (left) and V150(%) (right) of the DILs for all patients included in the study. In each case, the results are presented for the reference plan (target only), B1, B2 and B3.

Figure 6: Values of A) V50(cc) of the bladder, B) V50(cc) of the rectum, C) V120(cc) of the urethra for all patients included in the study. In each case, the results are presented for the reference plan, B1, B2 and B3.

Table I: Summary of patient population with DIL defined by MRS.

Table II: Dose constraints specified for the target (Prostate), three organs at risk (Bladder, Rectum and Urethra) and three levels of D.I.L. boosts, B1 (120% to 150%), B2 (150 to 150%) and B3 (150 to 170%).

Table III: Dosimetric indices of the organs at risk for the reference and 3 boost level plans. The average values of V50(cc) and V80(cc) are presented for the bladder and rectum. For the urethra, V120(cc) values are shown. The average relative increases over all patients of V50(%) (bladder, rectum) or V120(%) between the three boost levels (B1, B2 and B3) and the reference plan without boost are also presented. The numbers within brackets represent the standard deviation of the increases.

Table I

Summary of patient population with DIL defined by MRS

Patient #	Target Volume (cc)	DIL Volume (cc)			DIL/Target (%)
		Overall	Right lobe	Left Lobe	
1	36.5	5.15	0.52	4.63	14.1
2	31.7	3.24	1.17	2.07	10.2
3	36.2	2.50	2.50	0.78	6.9
4	32.2	5.84	4.22	1.63	18.1
5	30.7	3.00	2.02	0.98	9.8
6	39.1	3.93	irregular	irregular	10.1
7	31.6	3.42	1.53	1.89	10.8
8	34.0	4.76	1.82	2.94	14.0
9	44.7	2.44	2.01	0.43	5.5
10	37.5	1.99	0.00	1.99	5.3
Average	35.4	3.63			10.2

Table II: Dose constraints

Volume		Weight for D_{min}	D_{Min} (%)	D_{Max} (%)	Weight for D_{max}
PROSTATE Target	ON	100	100	150	100
	IN	100	100	150	30
DIL Target B1	ON	100	120	150	30
	IN	100	120	150	30
DIL Target B2	ON	100	150	150	30
	IN	100	150	150	30
DIL Target B3	ON	100	150	170	30
	IN	100	150	170	30
URETHRA Organ at risk	ON	100	100	120	30
	IN	100	100	120	30
BLADDER Organ at risk	ON	-	-	50	30
	IN	-	-	-	-
RECTUM Organ at risk	ON	-	-	50	30
	IN	-	-	-	-

Table III: Dosimetric indices for the reference and 3 boost level plans.

Boost Level	Bladder			Rectum			Urethra	
	V50 (cc)	Δ V50 (%) Boost - Ref	V80 (cc)	V50 (cc)	Δ V50 (%) Boost - Ref	V80 (cc)	V120 (cc)	Δ V120 (%) Boost - Ref
Ref	3.1		0.5	5.3		0.6	0.3	
B1	3.4	1.0 [1.1]	0.6	5.8	0.9 [0.6]	0.8	0.4	13.4 [9.8]
B2	3.5	1.3 [1.1]	0.6	6.5	2.8 [1.1]	1.1	0.5	32.0 [15.5]
B3	3.5	1.3 [1.1]	0.6	6.6	3.3 [1.2]	1.2	0.5	32.5 [14.8]
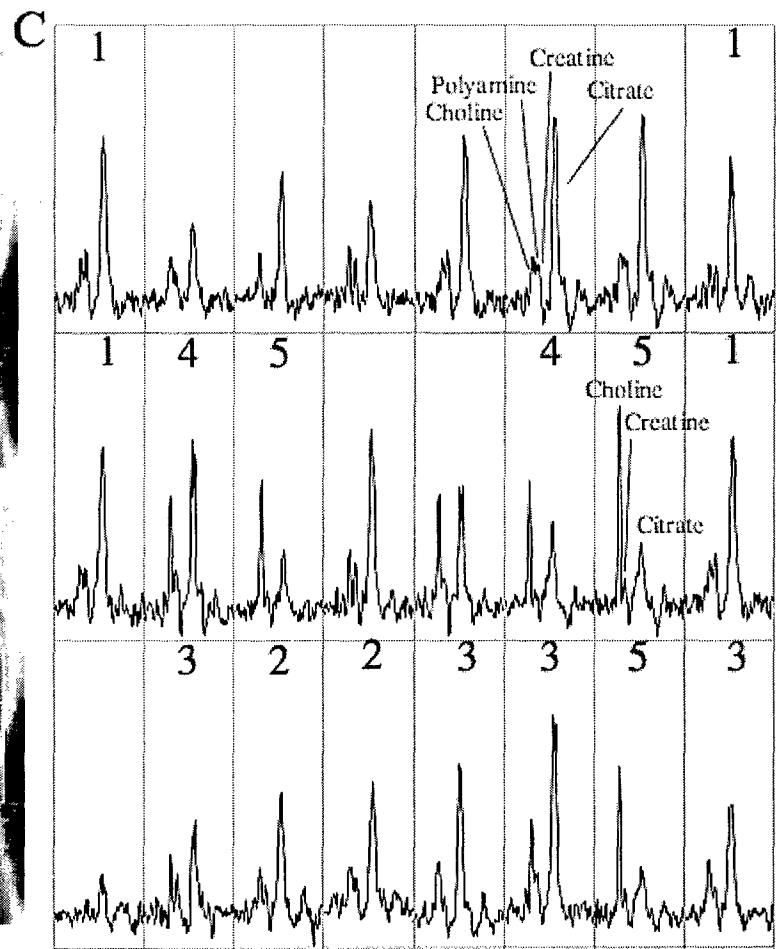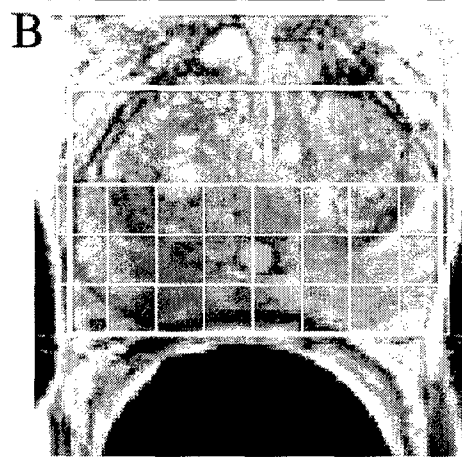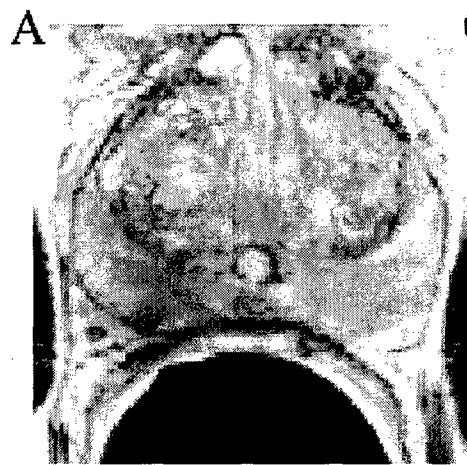
D
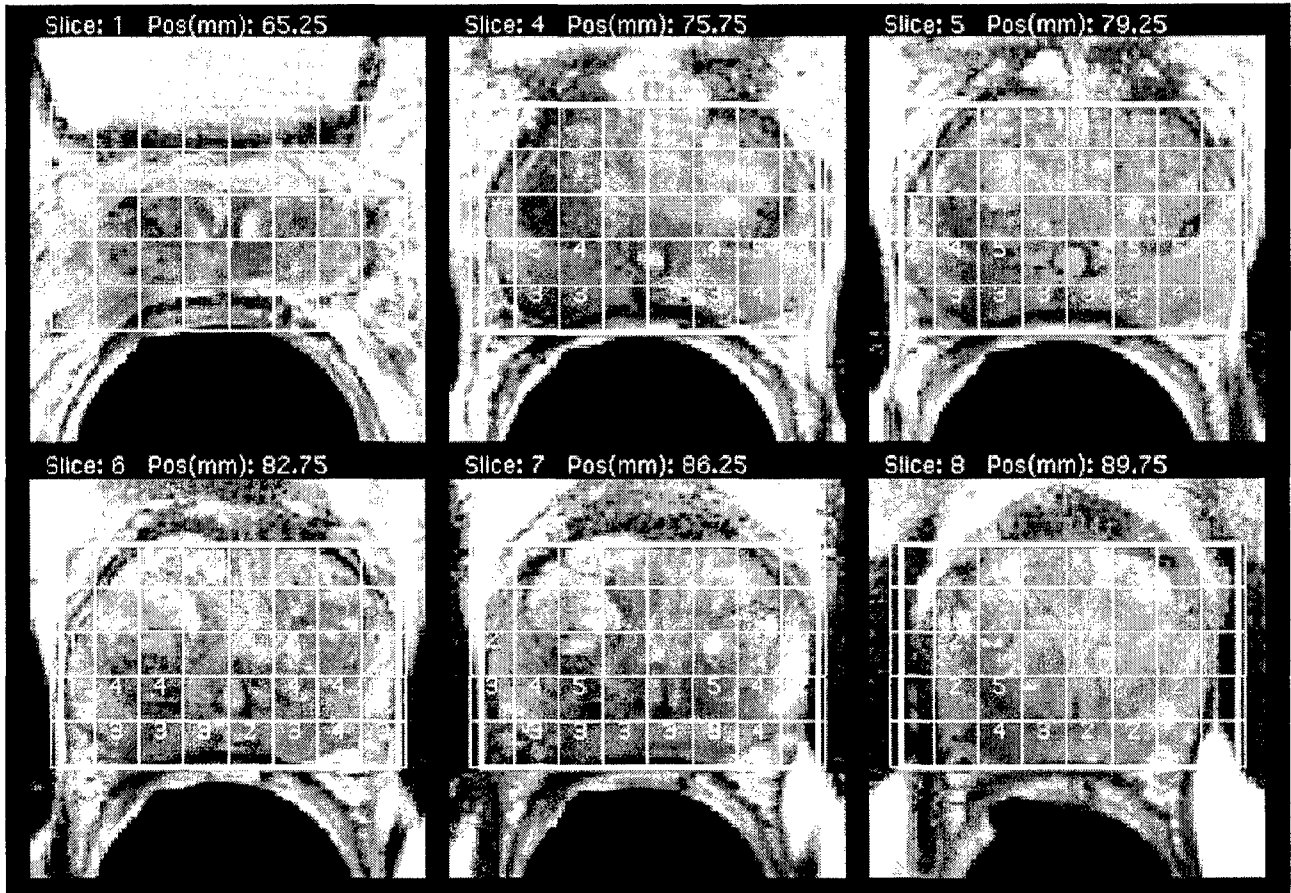
Figure 1, *Pouliot et al.*

(A)

(B)

(C)
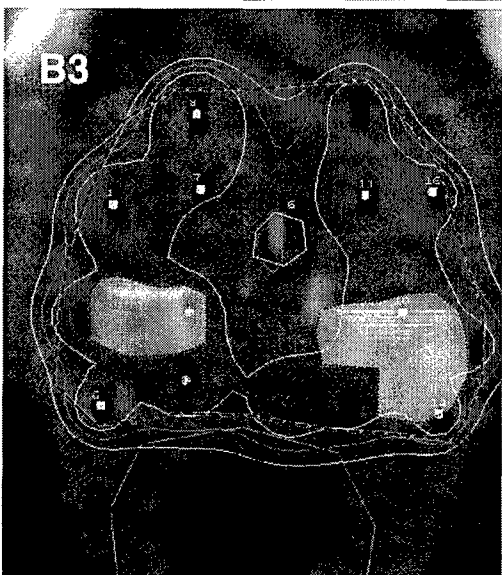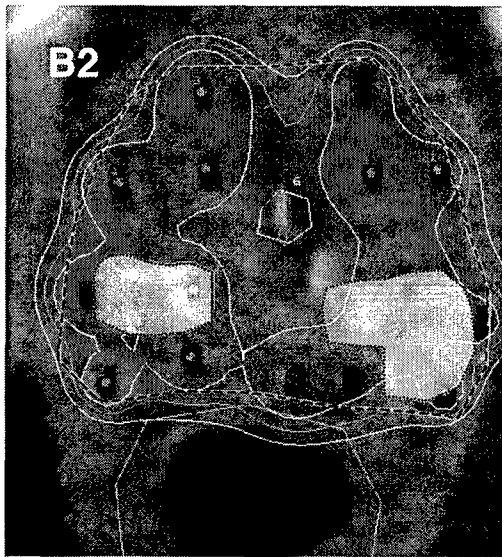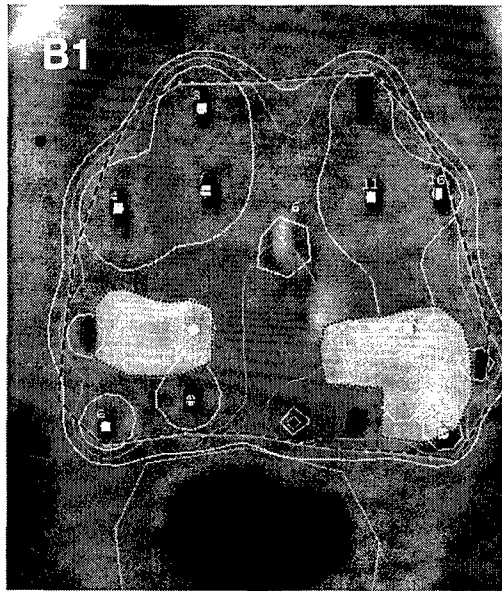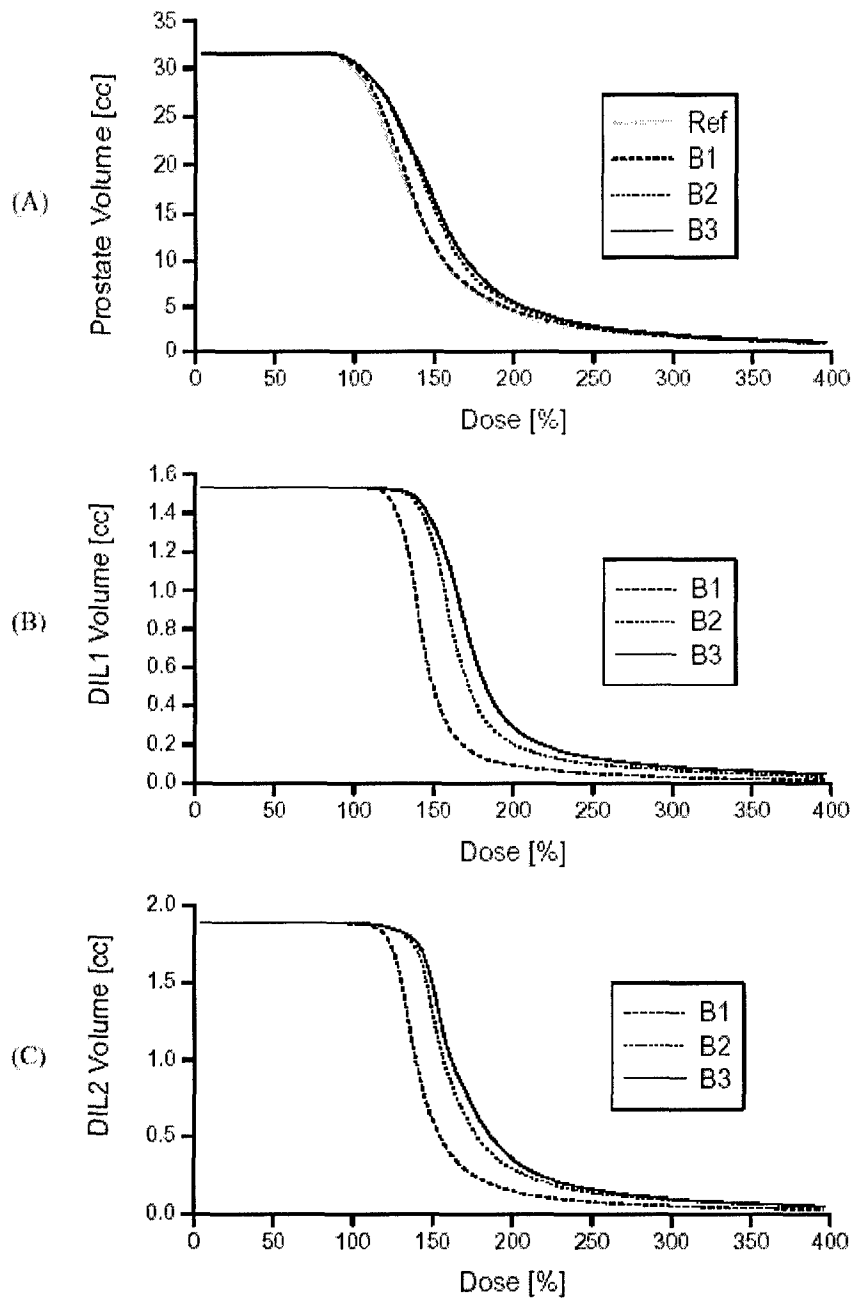
Figure 3, *Pouliot et al.*

(A)

(B)

(C)
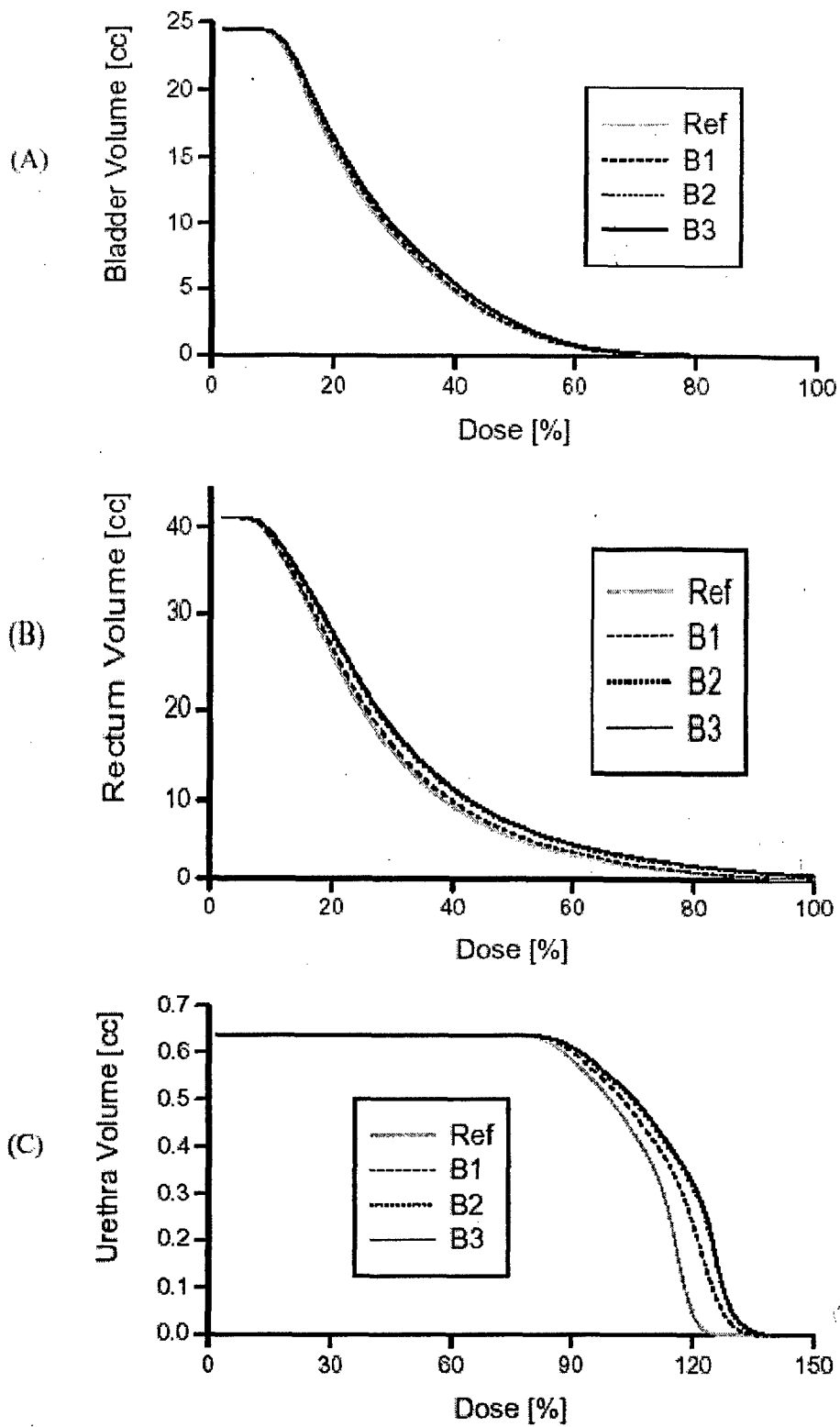
Figure 4, *Pouliot et al.*
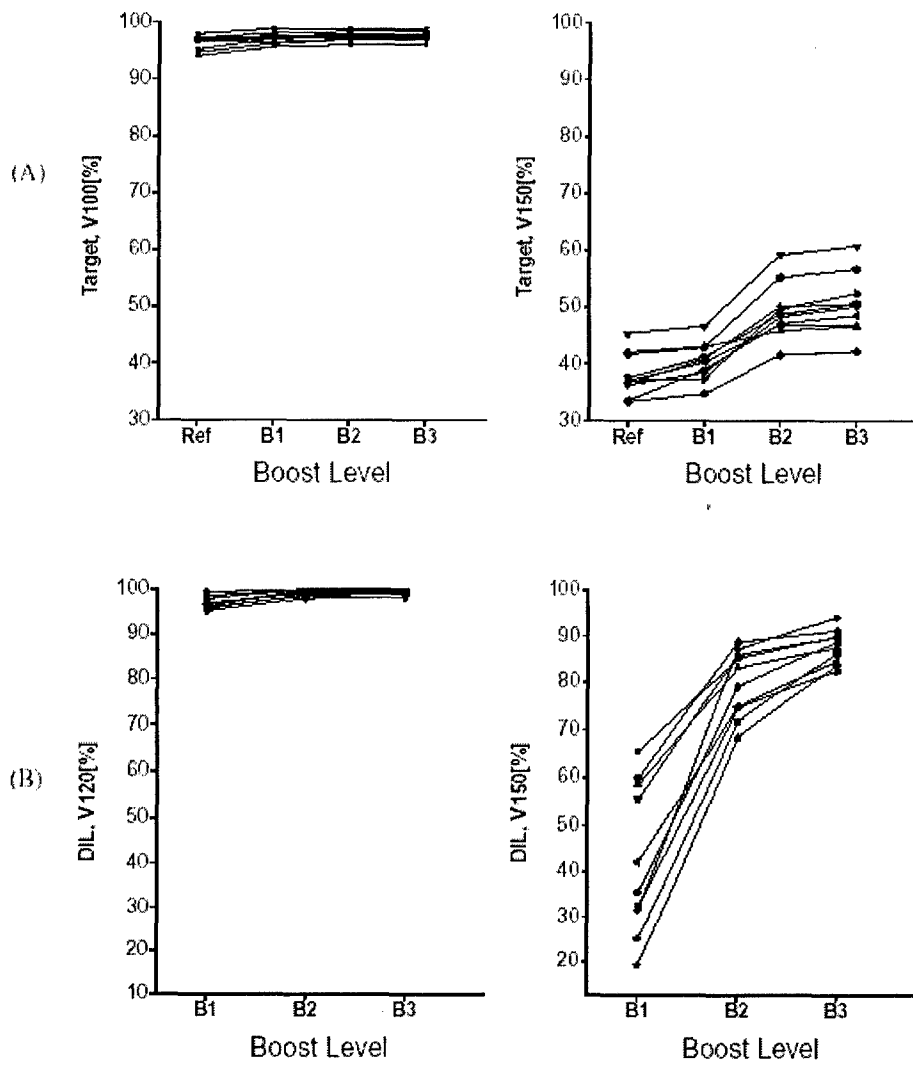
Figure 5, *Pouliot et al.*
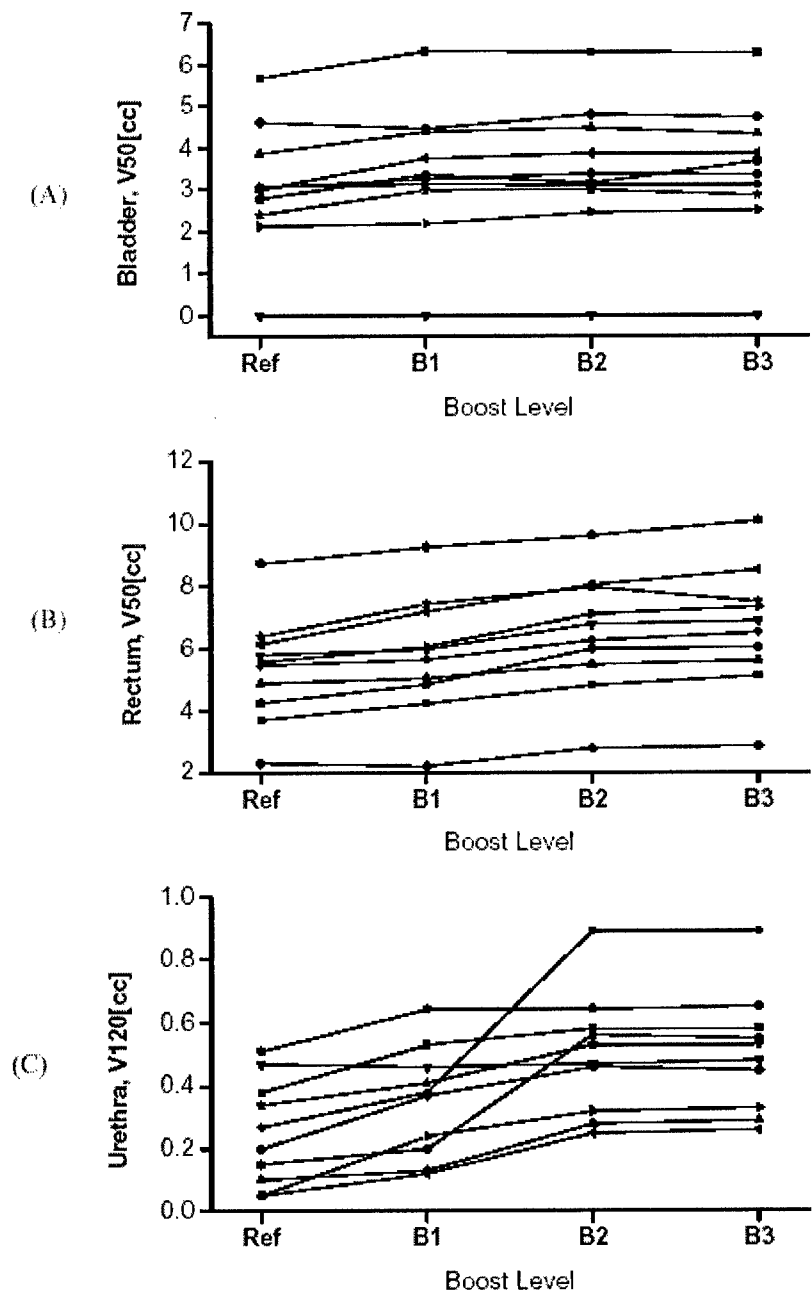
Figure 6, *Pouliot et al.*

Expandable and rigid endorectal coils for prostate MRI: Impact on prostate distortion and rigid image registration

Yongbok Kim, Susan Moyher Noworolski, Jean Pouliot, I-Chow J. Hsu, Daniel B. Vigneron, and John Kurhanewicz

Yongbok Kim, [a] I-Chow J. Hsu, and Jean Pouliot
Department of Radiation Oncology, University of California, San Francisco, Comprehensive Cancer Center, 1600 Divisadero Street, Suite H1031, San Francisco, CA 94143-1708

Susan Moyher Noworolski, Daniel B. Vigneron, and John Kurhanewicz
The Center for Molecular and Functional Imaging, Department of Radiology, University of California, San Francisco, 185 Berry Street, Suite 350, San Francisco, CA 94143-0946

[a] Author to whom correspondence should be addressed
UCSF Comprehensive Cancer Center
1600 Divisadero Street, Suite H1031
San Francisco, CA 94143-1708
Telephone: (415) 353-9849
Fax: (415) 353-9883
Electronic mail: kim@radonc17.ucsf.edu

Key words: Expandable endorectal coil, rigid endorectal coil, prostate distortion, rigid image registration, MRI

Running title: Impact of endorectal coils on prostate distortion

ABSTRACT

Endorectal coils (ERCs) are used for acquiring high spatial resolution magnetic resonance (MR) images of the human prostate. The goal of this study is to determine the impact of an expandable versus a rigid ERC on changes in the location and deformation of the prostate gland and subsequently on registering prostate images acquired with and without an ERC. Sagittal and axial T_2 weighted MR images were acquired from 25 patients receiving a combined MR imaging (MRI) /MR spectroscopic imaging (MRSI) staging exam for prostate cancer. Within the same exam, images were acquired using an external pelvic phased array coil both alone and in combination with either an expandable ERC (MedRad, Pittsburgh, PA) or a rigid ERC (USA Instruments, Aurora, OH). Rotations, translations and deformations caused by the ERC were measured and compared. The ability to register images acquired with and without the ERC using a manual rigid-body registration was assessed using a similarity index (SI). Both ERCs caused the prostate to tilt anteriorly with an average tilt of 18.5 degrees (17.4 ± 9.9 and 19.5 ± 11.3 degrees, mean ± standard deviation, for expandable and rigid ERC, respectively). However, the expandable coil caused a significantly larger distortion of the prostate as compared to the rigid coil; compressing the prostate in the anterior/posterior direction by 4.1 ± 3.0 mm versus 1.2 ± 2.2 mm (14.5% versus 4.8%) ($p < 0.0001$), and widening the prostate in the right/left direction by 3.8 ± 3.7 mm versus 1.5 ± 3.1 mm (8.3% versus 3.4%) ($p = 0.004$). Additionally, the ability to align prostate images acquired with and without ERC was significantly ($p < 0.0001$) better for the rigid coil (SI = 0.899 ± 0.033 versus 0.940 ± 0.008, for the expandable and rigid coils, respectively). In conclusion, the manual rigid-body alignment of prostate MR images acquired with and without the ERC can be improved through the use of a rigid ERC.

I. INTRODUCTION

Recent studies have demonstrated that the detection and characterization of prostate cancer can be improved by combining the anatomic and metabolic information provided by magnetic resonance imaging (MRI) and magnetic resonance spectroscopic imaging (MRSI) [1-8]. The combined prostate MRI and MRSI exam can be performed in less than an hour using a standard clinical 1.5 Tesla MRI scanner and commercially available coils, and MR vendors are offering or are close to releasing product versions of this exam. An expandable endorectal coil [9] (ERC) integrated into a pelvic phased array coil is commonly used for signal reception in the MRI/MRSI prostate exam due to the improved signal-to-noise ratio (SNR) and better spatial resolution MR images obtained as compared to using pelvic phased array coils alone [3-5]. The ERC is also critical for the acquisition of high spatial resolution (≈ 0.3 cc) MRSI data of the prostate due to the approximate 10-fold increase in SNR over the prostate provided by the ERC relative to external phased array coils [9]. Several recent studies have utilized MRI/MRSI data to identify the dominant regions of cancer inside the prostate for improved radiation treatment planning [10-14]. In particular, we used MRI/MRSI to escalate dose to selected regions inside the prostate without compromising the dose coverage of the prostate and the protection of the organs at risk for patients treated with high dose rate brachytherapy [12]. However, the displacement and distortion of the prostate caused by the ERC used in staging MRI/MRSI exams cause difficulties with alignment of the MRI/MRSI data to treatment planning CT or MRI images which are typically acquired without an ERC or to transrectal ultrasound planning images that employ an endorectal probe having a different shape. In addition to the commercially available expandable ERC, a number of rigid ERCs have also been designed and used for imaging and spectroscopic studies of the prostate [6-8]. The goal of this study is to determine the impact of an expandable versus a rigid ERC on changes in location and deformation of the prostate gland and subsequently on registering prostate images acquired with and without these ERCs.

II. METHODS AND MATERIALS

1. Patients cohorts

Twenty biopsy proven prostate cancer patients clinically referred for a combined MRI/MRSI staging exam between January and July of 2003 were studied. Five additional patients were enrolled between May and June of 2005 and therefore the total number of patients for this study was 25. The study was approved by our Committee on Human Research and informed consent was obtained from all patients. The patients had a mean Gleason score of 6.9 (6.6 for the rigid ERC patients versus 7.4 for the expandable ERC patients) and a mean age of 66 for each ERC group. The average volumes of the prostates were 31.4 cc, with a range from 15.1 to 47.7 cc for rigid ERC patients, and 42.3 cc, with range from 14.8 to 91.8 cc for expandable ERC patients. There were two large prostates, at 63.5 cc for patient Q and 91.8 cc for patient R. If the two patients with large prostates in the expandable ERC patient group are excluded, the mean prostate volume for the remaining 8 patients is 33.5 cc, similar to the rigid ERC patient group.

2. MRI protocol

Combined MRI/MRSI was obtained using either a rigid ERC (15 studies, refered to as A to O, USA Instruments, Aurora, OH) or an expandable ERC (10 studies, refered to as P to Y, MedRad, Pittsburgh) in combination with an external phased array of coils on a 1.5 Tesla GE system (Signa, GE Medical Systems, Milwaukee, WI). For rigid coil cases, the USA torso phased array was used, while the GE pelvic phased array was used for the expandable coil cases. Initially, no particular selection process was used to assign subjects to a coil configuration. During the course of this study, it was discovered that the rigid ERC gave less distortion than the expandable ERC and thus the rigid ERC became the coil used for all our radiation treatment planning prostate imaging examinations. Due to this protocol decision, initially only 5 subjects were studied with the expandable ERC whereas an additional 10, totaling 15, were studied with the rigid ERC. To improve comparison between the ERCs, an additional 5 subjects were studied with the expandable ERC, making the final numbers 15 for the rigid ERC and 10 for the expandable ERC.

The expandable coils, at 44 mm right/left (R/L) by 79 mm superior/inferior (S/I), were larger than the rigid coils at 22.5 mm R/L by 65mm S/I. The probes themselves also differed in size and shape. The expandable ERC had a circular cross-section, once inflated, with a 48 mm diameter. The rigid probe was a half ellipse, with the anterior surface flat. Its R/L extent was 29 mm and its anterior/posterior (A/P) extent was 16.5 mm. The S/I length of the expandable ERC probe (86 mm) was also longer than the rigid probe (82 mm).

The ERC images used in this study were acquired during a "PROSE" MRI/MRSI staging exam (GE Medical Systems, Milwaukee, WI) [15]. The details of the MR imaging technique have been previously described [12, 16-18]. In brief, patients were examined in the supine position, using the body coil for excitation and a combination of the ERC and pelvic phased array for signal reception. Thin-section high spatial resolution axial, coronal and sagittal T_2 weighted fast spin-echo images of the prostate and seminal vesicles were obtained using the following parameters: TR/effective TE = 5000/96 msec, echo train length = 16, slice thickness = 3 mm, inter-slice gap = 0 mm, field of view (FOV) = 14 cm, matrix 256 x 192, frequency direction antero-posterior (to prevent obscuration of the prostate by ERC motion artifact), and 3 excitations. The ERC was removed at the end of the staging MRI/MRSI exam with the subject remaining on the imaging table. Additional sagittal and axial fast spin echo T_2 weighted images were acquired without the ERC using the phased array coil alone for signal reception. As with the ERC, patients were scanned in the supine position. All imaging acquisition parameters were the same as for the ERC images except for increasing the FOV to 16 cm in order to compensate for the reduction in SNR obtained without the use of an ERC.

3. ERC induced changes in prostate location and shape

To assess the effect of the ERCs on the location and shape of the prostate, R/L, A/P, and S/I lengths and positions of the prostate were measured. Measurements were obtained on the MR images acquired with and without an ERC. The user modified the image intensity (window/level) settings to best depict the anatomy in

question. Such settings were not consistent within or across subjects due to the differences in signal of the images obtained with an ERC versus without and due to inter-patient variability. Prior to two-dimensional (2-D) image registration, the MR images acquired with and without the presence of ERCs were rotated to align the data into the same plane, approximately perpendicular to the long (superior-inferior) axis of the prostate. The amount of rotation was determined by the difference between the series angle and the prostate angle. The prostate angle was defined as the angle (_) between the line perpendicular to the axis of magnet bore and the long axis (S/I direction) of the prostate. The axial T_2 weighted prostate images in this study were often acquired obliquely in the S/I dimension in order to obtain true axial images through the prostate, and needed to be accounted for when calculating the prostate angle. This oblique angle was referred to as the series angle and was obtained from the series image header. The prostate angle was determined using T_2 weighted sagittal MR images taken at the middle of the prostate (Fig. 1). Three approaches (I, II and III) were used to draw a line along the superior-inferior direction of the prostate in order to define a long axis (S/I direction) of the prostate, and thus, the prostate angle. Three approaches were necessary due to the inability to clearly visualize the anterior and posterior surfaces of the prostate, the surgical pseudo-capsule and/or when there were dramatic changes in the A/P width of the prostate between the ERC in and ERC out acquisitions.

The three approaches use different methods to determine the long axis of the prostate. The angle between this line and the line perpendicular to the axis of magnet bore is then calculated as the prostate angle. Approach I worked for 17 out of the 25 studies (12 out of 15 for rigid ERCs and 5 out of 10 for expandable ERCs). In this approach, the long axis of the prostate was simply calculated based on drawing straight lines along the posterior and anterior surfaces of the prostate and determining the bisector of these lines (i. e. the average of the two angles) (Fig. 1(a) and 1(b)). Approach II was used for 6 studies (patients E, N, O for rigid ERCs and Q, R, U for expandable ERCs). In these cases, there was a greater than 10% increase in the A/P dimension of the prostate causing a large difference in the prostate angle determined using lines drawn along the posterior and anterior surfaces of the prostate. However, in these cases, the surgical pseudo capsule which separates the central gland from the peripheral zone was well visualized and a line drawn along the surgical pseudo capsule could be used to define the long axis of the prostate (Fig. (1c)). In the remaining two cases (patient P and T for expandable ERC), there was a more than 10% increase in the A/P dimension and the surgical pseudo capsule was not well visualized. In these cases (Approach III), the long axis of the prostate was calculated based on the average of the angle formed by the bisector of the anterior and posterior lines and the angle determined by the posterior line (Fig. 1 (d)). In each patient, the same approach was always taken for the case with an ERC and the case without an ERC. It is recognized that the three approaches may determine a different absolute angle, as they are based on different anatomical landmarks. However, the intent was to determine a procedure to consistently calculate the difference in rotation of the prostate when imaged with an ERC versus without an ERC. To evaluate the effect of the different approaches, all three approaches were performed in the patients for whom Approach I was possible.

In order to assess the change in position and shape of the prostate caused by the expandable and rigid ERCs, rotation in the sagittal plane (Rot_{Sag}), and translations ($T_{R/L}$, $T_{A/P}$, $T_{S/I}$), and deformations ($D_{R/L}$, $D_{A/P}$, $D_{S/I}$) along the R/L, A/P and S/I dimensions were determined. Rotations of the prostate in coronal and axial planes (Rot_{Cor}, Rot_{Axi}) were visually negligible. Changes in the prostate angle on ERC-in versus ERC-out cases were calculated and statistically compared for the ERCs (rigid and expandable) using a non-parametric test, Wilcoxon matched-pairs signed-rank test, and were subsequently used to rotate the prostate during image alignment.

The translations in the R/L and A/P dimensions ($T_{R/L}$, $T_{A/P}$) were measured in the axial plane since image registration between studies was performed in the axial plane. The translation in the S/I dimension ($T_{S/I}$) was determined by selecting a ERC-in axial MR image showing the same anatomy (ejaculatory ducts, urethra, benign prostatic hyperplasia nodules) as a ERC-out axial MR image.

Deformation of the prostate in the R/L and A/P dimensions ($D_{R/L}$, $D_{A/P}$) were determined by manually measuring the maximum R/L and A/P distances of the prostate between axial images acquired with and without the ERC. Two lateral location points of the prostate were visually selected to measure the maximum extent of the prostate in the approximate R/L and A/P dimensions. Hence, sometimes, the R/L and A/P

measures were not perfectly perpendicular, as in Fig. 3(c) and 3(d). The deformation of the prostate in the S/I dimension ($D_{S/I}$) was measured using the total number of axial images containing the prostate acquired with and without the ERC. Since deformation visually changed along the length of the prostate, separate deformation measurements were made using axial images taken from the prostatic base, midgland and apex.

4. Image registration

The ability to register images acquired with and without the ERC was determined using a manual rigid-body registration and assessed using a similarity index (SI) [19-20]. Two independent observers did the contouring and registration process for all patients to assess inter-observer differences on the calculated SI. To accomplish this, the contour of the prostate was manually drawn on each contiguous 2-D axial MR image forming a 3-D volume that was aligned between images acquired with and without the ERC. Prior to contouring the prostate, the contiguous 2-D MR images were stacked together to form a 3-D volume, and the volume was rotated in the sagittal plane by the difference in prostate angle after accounting for the series angle (Rot_{sag} = (MRI series angle – prostate angle) $_{ERC-in}$ – (MRI series angle – prostate angle) $_{ERC-out}$). Subsequently, the resolution (mm/pixel) of the ERC-in MR images was changed to equal that of the ERC-out MR images and the ERC in and ERC out images were visually aligned in the S/I dimension based on the anatomy of the prostate. Finally, contours were manually drawn on the 2-D images outlining the prostate, and the contoured ERC-in volume was translated in the R/L and A/P directions, based on the mean value of the R/L and A/P coordinates of the contoured ERC-out volume.

The exactness of image registration between ERC in and ERC out contoured volumes was evaluated using a SI value. The SI value (ranging from 0 to 1) was defined as the ratio of twice the common area (A ∩ B) to the sum of the individual areas (A + B). For example, if the contoured volumes were perfectly matched, the SI value would be 1, whereas no overlap would result in a SI value of 0.

$$SI = \frac{2\{A \cap B\}}{A + B} = \frac{2c}{a + b + 2c}$$

Where 'A' and 'B' are the two contoured volumes, 'a' is the area belonging to only contour volume 'A', 'b' is the area occupied by only contoured volume 'B', and 'c' is the overlapping region between volumes 'A' and 'B'.

III. RESULTS

1. Impact of ERC on prostate location

There were 17 cases in which the increase in A/P dimension was less than 10%, and thus, Approach I for determining the prostate angle could be applied. All three approaches described in Section II.3 were performed in these subjects and summarized in Table II. As described in the methods, these approaches measure the prostate angle differently and thus, determine different angles. For a prostate, the prostate angle is significantly different depending on which approach was employed ($p < 0.0001$ by Friedman test, nonparametric repeated measures ANOVA) and, in general, the largest angle is measured by approach I, the second by approach III (6.4 ± 3.6 degrees less than Approach I), and the smallest by approach II (13.2 ± 8.0 degrees less than Approach I). The prostate angles determined for each subject were used to rotate the ERC in and ERC out image data into the same plane. For this, the difference in angle between ERC-in and ERC-out studies is of primary relevance and was not significantly different for the three approaches ($p = 0.1134$ by Friedman test). The mean ± standard deviation value of the angle difference were 20.0±11.4, 19.7±9.8 and 21.8±11.3 for Approaches I, II and III, respectively.

Figure 2 summarizes the changes in prostate angle between ERC-in and ERC-out studies for the 25 patient studies (15 rigid coil studies, and 10 expandable coil studies). As observed in Figure 2, both ERCs (Fig. 2(a) – rigid coil, Fig. 2(b) – expandable coil) caused the superior portion of the prostate to tilt anteriorly

with an average angle of 18.5 degrees. Specifically, the mean angle change between ERC-in and ERC-out was 19.5 degrees for the rigid coil, and 17.4 degrees for the expandable coil.

2. Impact of ERC on prostate deformation

As can be seen in comparing Fig. 1(a) with Fig. 1(b), the presence of the rigid ERC did not affect the S/I length of prostate as compared to the images acquired without the ERC. Quantitatively, the difference in the S/I length of the prostate measured between images acquired with and without either ERC was always less than the thickness of an axial MR image (3 mm).

Figure 3 shows representative axial MR images taken from the midgland of two patients acquired with (a) and without (b) the expandable ERC and with (c) and without (d) the rigid ERC, respectively. Visually, it is apparent from Fig. 3 that the expandable ERC distorted the prostate to a greater degree in both the R/L and A/P dimensions as compared to the rigid ERC. Quantitatively, the prostate was 0.51 cm (12.8%) larger in the R/L dimension when using the expandable coil (4.50 versus 3.99 cm) and only 0.12 cm (3%) larger when using the rigid coil (4.19 versus 4.07 cm). In the A/P dimension, the prostate was compressed by 0.23 cm (7.5%) for the expandable coil (2.84 versus 3.07 cm), while it was negligibly different for the rigid coil, 0.05 cm (2%) (2.51 versus 2.56 cm).

Figure 4 graphically summarizes the A/P (a) and R/L (b) distortions for the rigid (squares) and expandable (circles) ERCs at the base, midgland and apex of the prostate, with the numerical values reported in Table I. Similar to the representative cases shown in Fig. 3, on average the expandable coil caused a significantly larger distortion of the prostate as compared to the rigid coil; compressing the prostate in the A/P direction by 4.1 ± 3.0 mm (mean $\pm$ standard deviation) versus 1.2 ± 2.2 mm (14.5% versus 4.8%) ($p <$ 0.0001), and widening the prostate in the R/L direction by 3.8 ± 3.7 mm versus 1.5 ± 3.1 mm (8.3% versus 3.4%) ($p = 0.004$). Additionally, the expandable coil consistently caused larger distortions along the S/I length of the prostate (base, midgland and apex of gland) as compared to the rigid coil, with the distortions being significantly larger ($P < 0.05$) at all locations except for the A/P dimension at the midgland and the R/L dimension at the base and apex of prostate due to the large variability of theses measurements (Fig. 4(a) and 4(b)). There was no significant difference in the degree of deformation with location (apex, midgland and base) for either ERC.

3. Registration of images acquired with and without ERC

Figure 5 shows representative cases (at the base, midgland and apex of prostate) of the quality of image registration attained after rotations and translations for a rigid coil case (Fig. 5(a)) and an expandable coil case (Fig. 5(b)). It is visually clear that the registration of images acquired with and without the expandable coil (Fig. 5(b)) is not as good as the registration of images with and without the rigid coil (Fig. 5(a)) due to the larger A/P and R/L distortions caused by the expandable coil. Figure 6 graphically demonstrates the improvement in the similarity index attained using the rigid coil. Quantitatively, the ability to align prostate images acquired with and without ERC was significantly ($p < 0.0001$) better for the rigid coil (SI = 0.941 ± 0.008, range from 0.925 to 0.952) than for the expandable coil (SI = 0.899 ± 0.033, range from 0.812 to 0.928). In addition, the average difference of SI values calculated by two different observers is 0.0059 with maximum difference of 0.01972. There was no significant difference between the two observers (p-value is 0.3525 using Wilcoxon matched-pairs signed-ranks test) in obtaining SI values using rigid image registration between ERC-in and ERC-out MR images. However, each prostate contour for a prostate is different to a certain extent depending on each observer.

IV. DISCUSSION AND CONCLUSION

Recently, there have been a number of published approaches [20-30] for the alignment of high spatial resolution prostate MRI and in some cases MRSI data acquired using an ERC with ultrasound, CT or MR radiation treatment planning images acquired without the use of the ERC or with a differently shaped transrectal ultrasound probe. A majority of these studies utilized a commercially available expandable ERC

for MR acquisition [20, 25-30]. However, at least two studies [23-24] employed a rigid ERC for the acquisition of the MRI/MRSI data. In this study we demonstrate that while both types of ERCs similarly displace the prostate, the use of a rigid coil significantly reduces the deformation of the prostate, allowing for more accurate image registration using a manual rigid-body approach.

Specifically, we found that both rigid and expandable ERCs caused the prostate to tilt anteriorly with an average of 18.5 degrees in the sagittal plane. This rotation changed the position of the prostate relative to the surrounding anatomy (pubic symphysis, ischial bone, rectum, bladder and so forth), making the use of external anatomy inaccurate for the registration of the ERC prostate images to treatment planning images. Therefore the approach taken was to use the prostate itself for registration of the imaging data. However, prior to registering the ERC images to the treatment planning images, the ERC images needed to be corrected for the anterior tilt of the prostate.

Neither ERC caused a significant change in the S/I length of the prostate. Hirose et al. [31] also observed a negligible deformation (median of 1.5 mm) in the S/I dimension between pre-operative and intraoperative MR prostate images. However, in this study the expandable ERC caused both a 3.5-fold larger compression of the prostate in the A/P direction, and a 2.5-fold larger widening of the prostate in the R/L direction as compared to the rigid ERC. In the study by Hirose et al. [31], the expandable ERC caused a mean decrease of 4.9 mm in the A/P dimension and 4.5 mm widening in R/L dimension that were close to the values reported in this study (4.1 mm and 3.8 mm). A possible explanation for the small difference in gland distortion between the two studies was that the non-ERC images in the Hirose et al. study [31] were acquired with a rectal obturator typically used during brachytherapy to fix the prostate. For both ERCs there was no significant difference in the degree of deformation with S/I location of prostate (apex, midgland and base).

The larger distortion of the prostate induced by the expandable ERC resulted in poorer rigid image registration as reflected by a significantly reduced similarity index (0.899 ± 0.033) than that obtained for the rigid coil (0.94 ± 0.008). Although the registration performed in this study involved only manual rotations and translations without any correction for deformation, the mean SI value obtained for the rigid ERC (0.94, 95% confidence interval (CI): 0.937 – 0.946) was identical to a prior study involving 3-D image registration using biomechanical finite element model for the registration of expandable ERC in and ERC out images (0.94, 95% CI: 0.89-0.99) [20]. However, that study involved subjects scanned in two different positions, supine and lithotomy, which may have also contributed to gland distortion and poorer image registration. Since the major deformation of the prostate was observed in the axial plane, it is likely that performing a rigid rotation prior to a 2-D deformable alignment such as B-spline [25] or finite element method [20, 24, 27] would likely further improve registration of rigid ERC images.

The larger distortion of the prostate induced by the expandable ERC resulted in poorer rigid image registration as reflected by a significantly reduced similarity index (0.899 ± 0.033) than that obtained for the rigid coil (0.94 ± 0.008). Although the registration performed in this study involved only manual rotations and translations without any correction for deformation, the mean SI value obtained for the rigid ERC (0.94, 95% confidence interval (CI): 0.937 – 0.946) was identical to a prior study involving 3-D image registration using biomechanical finite element model for the registration of expandable ERC in and ERC out images (0.94, 95% CI: 0.89-0.99) [20]. However, that study involved subjects scanned in two different positions, supine and lithotomy, which may have also contributed to gland distortion and poorer image registration.

In the current study, there was deformation of the prostate, primarily in the axial plane. Thus, a method to improve upon our current rigid image registration might be to first perform a rigid body rotation as we have done, but then apply a 2D deformable alignment such as B-spline [25] or finite element method [20, 24, 27] in the axial plane. Further improvements might be obtained with a 3D deformable technique such as in Bharatha et al. [20] Such approaches will need to be investigated further and compared to evaluate the benefits and drawbacks of the individual methods for this population.

One concern of the current study is that two of the expandable ERC subjects had unusually large prostates (63.5 cc and 91.8 cc versus the remaining mean = 33.5 cc). Calculating expandable ERC distortions and the SI from image registration with or without these cases did not have a significant effect on the results. Without these two subjects, the R/L expansion of the prostate remained the same, at 8.3%, and

the A/P compression was slightly and insignificantly less, at 12.6% ± 2.3 (versus 14.5% ± 2.4 with all expandable ERC subjects). These distortions were still significantly larger than those with the rigid ERC. When removing the large prostate cases, the mean SI value for the expandable ERCs remained at 0.897, indicating the negligible effect of the prostate size on rigid image registration, at least for these two large prostate cases.

The current study has several limitations due to the manual nature of the registration procedures used, including: (1) the definition of the prostate angle is sensitive to the experience of the reader, (2) the contouring of the prostate gland from images acquired without an ERC had an intrinsic uncertainty due to poorer image quality, and (3) the contouring of the prostate from 2-D images acquired with and without an ERC suffers from the fact that the image slices are not at the exact same anatomical locations within the prostate.

In conclusion, both rigid and expandable ERC caused a significant anterior tilt of the superior aspect of the prostate in the sagittal plane and it is important to correct for this rotation when registering images acquired with and without an ERC. The rigid ERC induced significantly less deformation of the prostate in the R/L and A/P dimensions than the expandable ERC leading to better rigid image registration of images acquired with and without an ERC.

REFERENCES

1. M. D. Schnall, R. E. Lenkinski, H. M. Pollack, Y. Imai and H. Y. Kressel, "Prostate: MR imaging with an endorectal surface coil," Radiology **172**, 570-574 (1989).
2. H. Hricak, S. White, D. Vigneron, J. Kurhanewicz, A. Kosco, D. Levin, J. Weiss, P. Narayan and P. R. Carroll, "Carcinoma of the prostate gland: MR imaging with pelvic phased-array coils versus integrated endorectal--pelvic phased-array coils," Radiology **193**, 703-709 (1994).
3. C. E. Hayes, M. J. Dietz, B. F. King and R. L. Ehman, "Pelvic imaging with phased-array coils: quantitative assessment of signal-to-noise ratio improvement," J. Magn. Reson. Imaging **2**, 321-326 (1992).
4. J. E. Husband, A. R. Padhani, A. D. MacVicar and P. Revell, "Magnetic resonance imaging of prostate cancer: comparison of image quality using endorectal and pelvic phased array coils," Clin. Radiol. **53**, 673-681 (1998).
5. D. J. Gilderdale, N. M. deSouza, G. A. Coutts, M. K. Chui, D. J. Larkman, A. D. Williams and I. R. Young, "Design and use of internal receiver coils for magnetic resonance imaging," Br. J. Radiol. **72**, 1141-1151 (1999).
6. N. M. deSouza, D. J. Gilderdale, R. Puni, G. A. Coutts and I. R. Young, "A solid reusable endorectal receiver coil for magnetic resonance imaging of the prostate: design, use, and comparison with an inflatable endorectal coil," J. Magn. Reson. Imaging **6**, 801-804 (1996).
7. P. Narayan, D. B. Vigneron, P. Jajodia, C. M. Anderson, M. W. Hedgcock, E. A. Tanagho and T. L. James, "Transrectal probe for 1H MRI and 31P MR spectroscopy of the prostate gland," Magn. Reson. Med. **11**, 209-220 (1989).
8. J. Kurhanewicz, A. Thomas, P. Jajodia, M. W. Weiner, T. L. James, D. B. Vigneron and P. Narayan, "31P spectroscopy of the human prostate gland in vivo using a transrectal probe," Magn. Reson. Med. **22**, 404-413 (1991).
9. J. Kurhanewicz, M. G. Swanson, S. J. Nelson and D. B. Vigneron, "Combined magnetic resonance imaging and spectroscopic imaging approach to molecular imaging of prostate cancer," J. Magn. Reson. Imaging **16**, 451-463 (2002).
10. S. J. DiBiase, K. Hosseinzadeh, R. P. Gullapalli, S. C. Jacobs, M. J. Naslund, G. N. Sklar, R. B. Alexander and C. Yu, "Magnetic resonance spectroscopic imaging-guided brachytherapy for localized prostate cancer," Int. J. Radiat. Oncol. Biol. Phys. **52**, 429-438 (2002).
11. B. Pickett, E. Vigneault, J. Kurhanewicz, L. Verhey and M. Roach, "Static field intensity modulation to treat a dominant intra-prostatic lesion to 90 Gy compared to seven field 3-dimensional radiotherapy," Int. J. Radiat. Oncol. Biol. Phys. **44**, 921-929 (1999).
12. J. Pouliot, Y. Kim, E. Lessard, I. C. Hsu, D. B. Vigneron and J. Kurhanewicz, "Inverse planning for HDR prostate brachytherapy used to boost dominant intraprostatic lesions defined by magnetic resonance spectroscopy imaging," Int. J. Radiat. Oncol. Biol. Phys. **59**, 1196-1207 (2004).
13. M. Zaider, M. J. Zelefsky, E. K. Lee, K. L. Zakian, H. I. Amols, J. Dyke, G. Cohen, Y. Hu, A. K. Endi, C. Chui and J. A. Koutcher, "Treatment planning for prostate implants using magnetic-resonance spectroscopy imaging," Int. J. Radiat. Oncol. Biol. Phys. **47**, 1085-1096 (2000).
14. M. J. Zelefsky, G. Cohen, K. L. Zakian, J. Dyke, J. A. Koutcher, H. Hricak, L. Schwartz and M. Zaider, "Intraoperative conformal optimization for transperineal prostate implantation using magnetic resonance spectroscopic imaging," Cancer J. **6**, 249-255 (2000).
15. "Signa® LX Release 9.1", Chap 6. PROSE Pulse Sequence, 2333956-100 Rev. 0 (05/02), General Electric Company (2002).
16. J. Kurhanewicz, D. B. Vigneron, H. Hricak, P. Narayan, P. Carroll and S. J. Nelson, "Three-dimensional H-1 MR spectroscopic imaging of the in situ human prostate with high (0.24-0.7-cm3) spatial resolution," Radiology **198**, 795-805 (1996).

17.   T. K. Tran, D. B. Vigneron, N. Sailasuta, J. Tropp, P. Le Roux, J. Kurhanewicz, S. Nelson and R. Hurd, "Very selective suppression pulses for clinical MRSI studies of brain and prostate cancer," Magn. Reson. Med. **43**, 23-33 (2000).

18   A. A. Schricker, J. M. Pauly, J. Kurhanewicz, M. G. Swanson and D. B. Vigneron, "Dualband spectral-spatial RF pulses for prostate MR spectroscopic imaging," Magn. Reson. Med. **46**, 1079-1087 (2001).

19.   A. P. Zijdenbos, B. M. Dawant, R. A. Margolin, and A. C. Palmer, "Morphometric analysis of white matter lesions in MR images: Method and validation," IEEE Trans. Med. Imaging. **13,** 716–724 (1994).

Table I. The mean ± standard deviation A/P (A) and R/L (B) distortions for the ERCs at the base, midgland and apex of the prostate. Significance between the ERC's is listed, based on Mann-Whitney rank-sum test.

(A) A/P distance decrease between ERC-in versus ERC-out studies (unit is mm)

S/I Region of Prostate	Type of ERC	Mean (relative change)	Standard Deviation
Base (p = 0.0115)	15 Rigid cases	1.60 (4.9%)	2.22
	10 Expandable cases	4.1 (13.2%)	2.17
Mid (p = 0.0593)	15 Rigid cases	1.17 (3.7%)	2.73
	10 Expandable cases	3.82 (13.0%)	3.22
Apex (p = 0.0163)	15 Rigid cases	0.81 (3.1%)	1.77
	10 Expandable cases	4.36 (17.2%)	3.58

(B) R/L distance increase between ERC-in versus ERC-out studies (unit is mm)

S/I Region of Prostate	Type of ERC	Mean (relative change)	Standard Deviation
Base (p = 0.0709)	15 Rigid cases	1.45 (4.2%)	3.39
	10 Expandable cases	3.76 (7.7%)	3.74
Mid (p = 0.023)	15 Rigid cases	1.61 (4.3%)	3.29
	10 Expandable cases	3.94 (8.3%)	2.73
Apex (p = 0.2852)	15 Rigid cases	1.42 (4.2%)	2.73
	10 Expandable cases	3.55 (9.0%)	4.66

Table II. Comparison of long axes of the prostate measured by three different approaches (approach I, II, and III mentioned in Section II.3) for 17 patients. Unit is degrees.

	Approach (ERC-in)			Approach (ERC-out)			Angle Difference (ERC-in) – (ERC-out)		
	I	II	III	I	II	III	I	II	III
Mean	106.3	93.2	100.8	86.3	73.5	79.0	20.0	19.7	21.8
*SD	9.9	7.9	10.1	17.9	13.8	17.1	11.4	9.8	11.3
Median	106.1	93.7	101.8	86.6	71.3	79.6	17.7	18.8	20.6
Minimum	86.3	77.8	75.7	51.5	44.9	47.7	1.8	4.1	0.7
Maximum	129.9	104.8	121.7	128.1	99.0	121.0	42.9	42.5	45.1
95% **CI (From)	101.2	89.2	95.6	77.1	66.4	70.2	14.1	14.6	16.0
95% **CI (To)	111.4	97.3	106.0	95.6	80.7	87.8	25.8	24.7	27.6

*SD: Standard Deviation, **CI: Confidence Interval

Figure Captions

Figure 1. T_2 weighted sagittal MR images illustrating the three approaches used to determine the prostate angle: Approach I was used for (a) and (b), approach II for (c), and approach III for (d). The anterior/posterior (A/P) distance (dashed line in the A/P direction) was 2.96, 3.22, 3.45 and 2.71 cm for (a), (b), (c) and (d), respectively. The prostate angle (_, curved dashed arrow) was measured counterclockwise between the prostate S/I axis (PA) and the line perpendicular to the axis of magnet bore (expressed with a dot straight arrow). The prostate angle was 106.1, 90.2, 91.5 and 114.5 degrees, for (a), (b), (c) and (d), respectively. In figures (a), (b), (d), the straight line along the anterior and posterior surface of the prostate is defined as AL and PL, respectively. In figure (c), CG and PZ stand for central gland and peripheral zone of the prostate. In figure (d), BL means the bisector line between AL and PL.

Figure 2. Summary of the changes in prostate angle between ERC-in and ERC-out studies for the (a) 15 rigid ERC studies (A to O) and (b) 10 expandable ERC studies (P to Y).

Figure 3. Representative axial MR images taken from the midgland of two patients acquired with (a) and without (b) the expandable ERC and with (c) and without (d) the rigid ERC, respectively. The R/L distance is 4.50, 3.99, 4.07 and 4.19 cm for (a), (b), (c) and (d), respectively. The A/P distance is 2.84, 3.07, 2.51 and 2.56 cm for (a), (b), (c) and (d), respectively.

Figure 4. Graphical summary of the A/P (a) and R/L (b) distortions for the rigid (squares) and expandable (circles) ERCs at the base, midgland and apex of the prostate. Error bar graphs show mean ± standard deviations.

Figure 5. Representative cases demonstrating the quality of image registration attained after rotations and translation for a rigid coil case (Fig. 5(a)) and an expandable coil case (Fig. 5(b)). Gray regions are the prostate contours from axial MR images acquired without ERC and white line contours are the prostate contours from axial MR images acquired with ERC. Three axial MR slices were obtained at the base ((a1), (b1)), midgland ((a2), (b2)) and apex ((a3), (b3)) of prostate. The SI values are 0.952 (a) and 0.905 (b).

Figure 6. Comparison of the rigid image registration between rigid and expandable ERC using similarity index (SI). Each parallel bar in the box graph represents minimum, 25, 50, 75 percentiles and maximum values in order and the dot inside the box is the mean value.
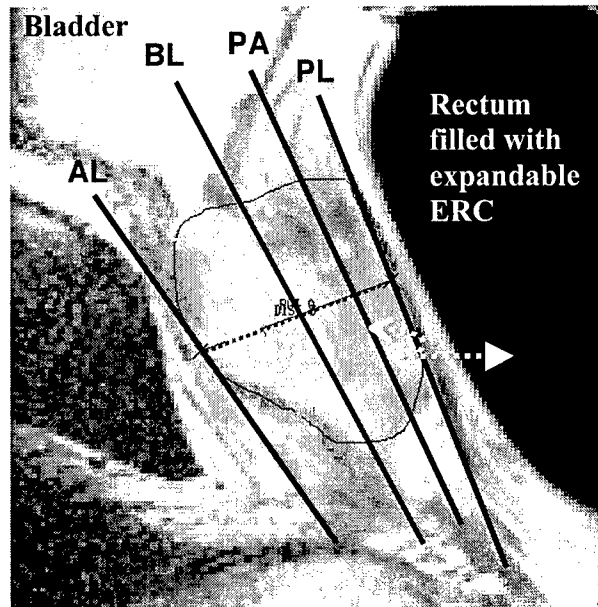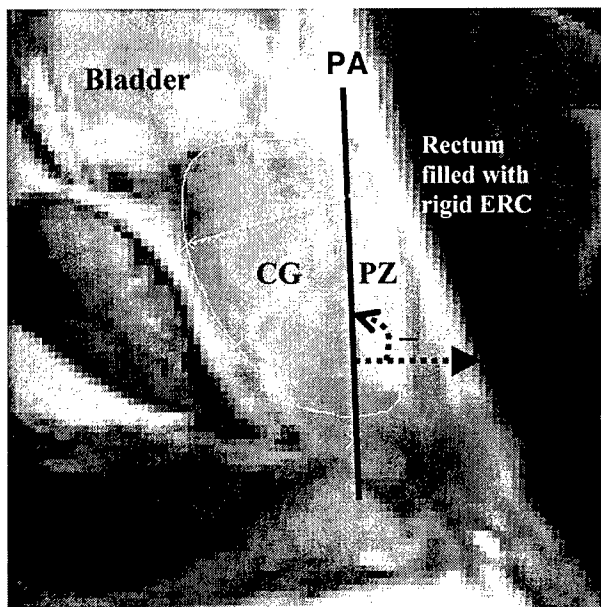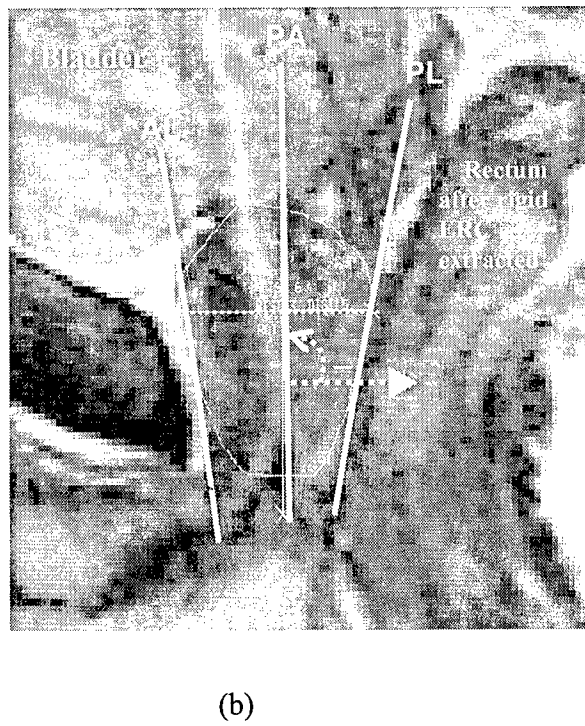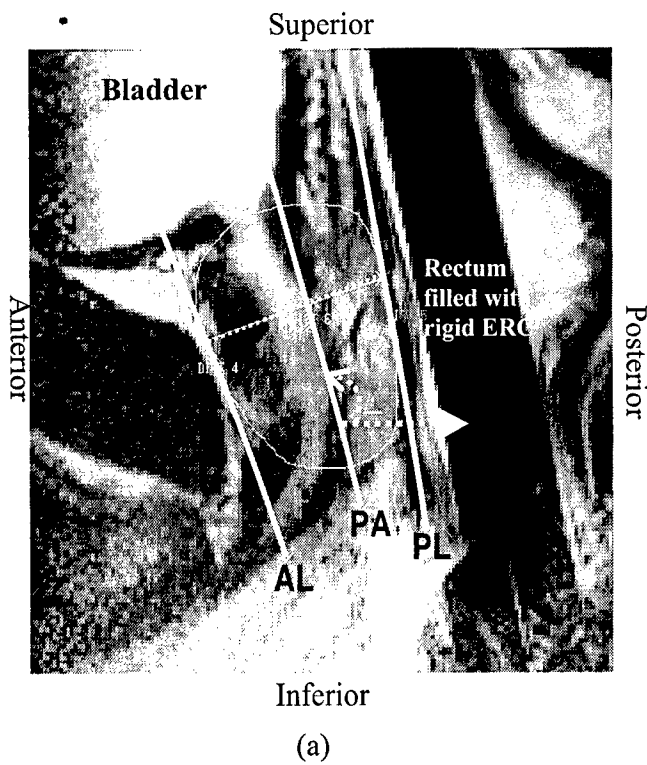
Figure 1. *Kim et al.,* Impact of endorectal coils on prostate distortion
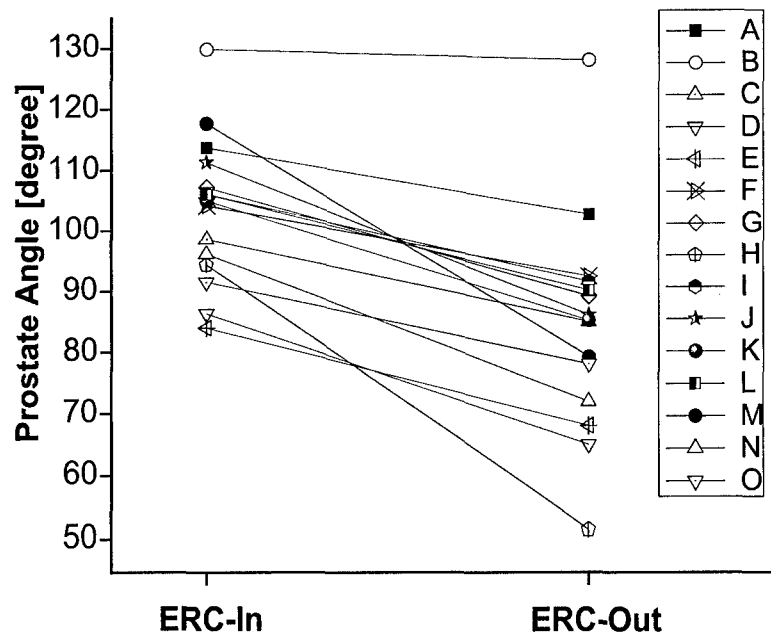
(a)
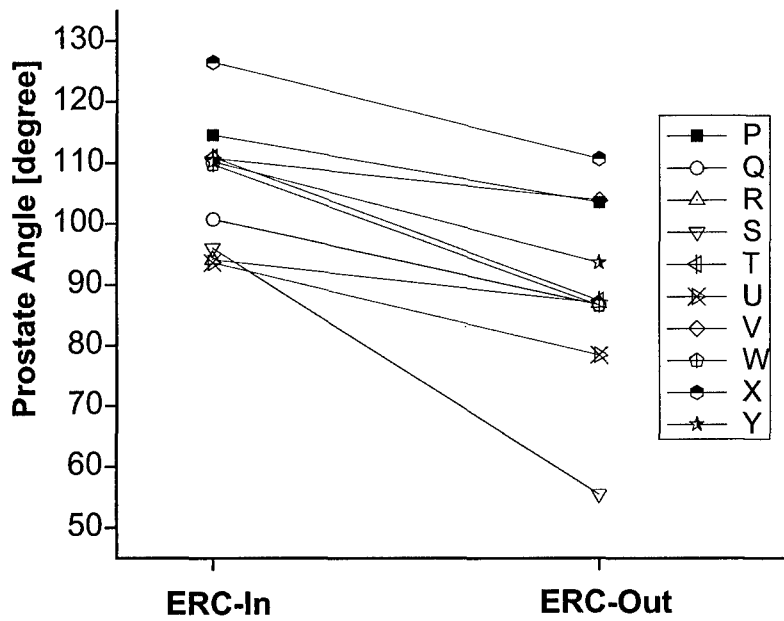
(b)

Figure 2. *Kim et al.,* Impact of endorectal coils on prostate distortion
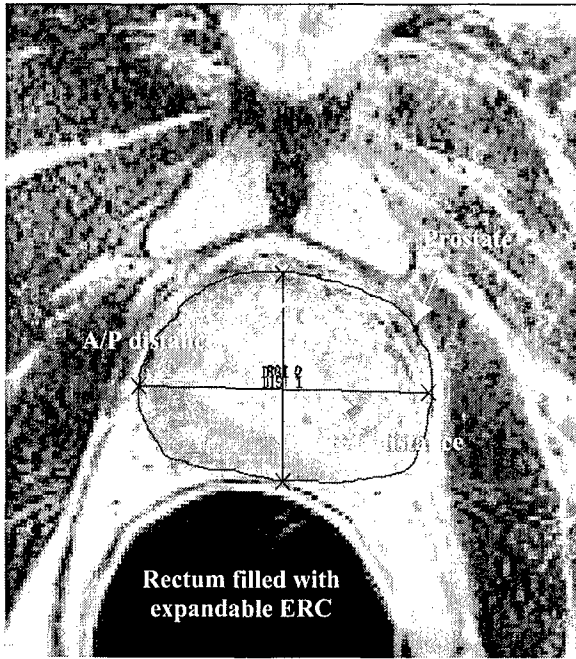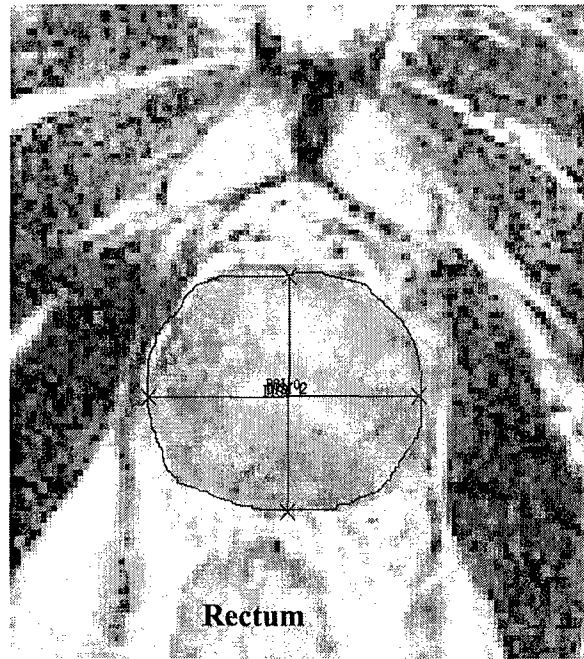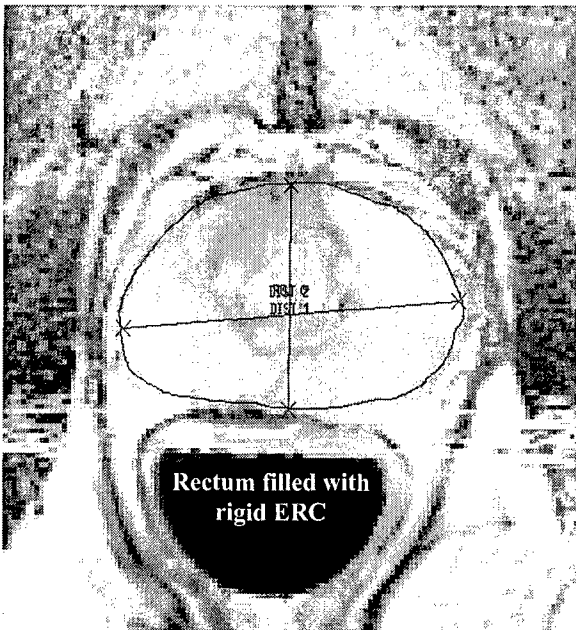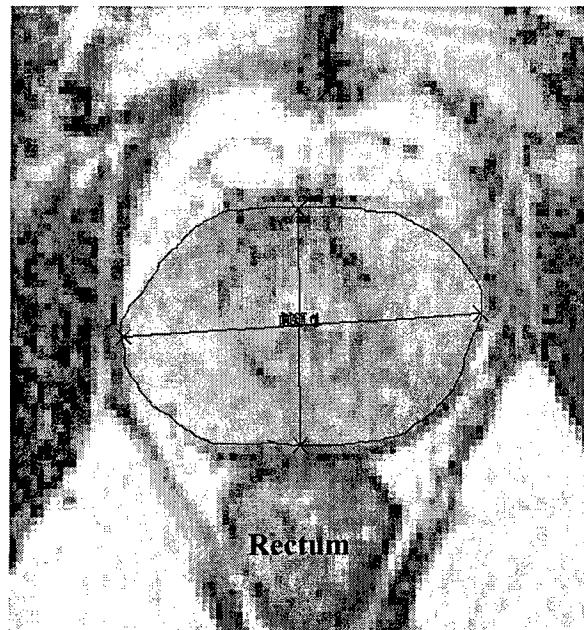
Figure 3. *Kim et al.,* Impact of endorectal coils on prostate distortion
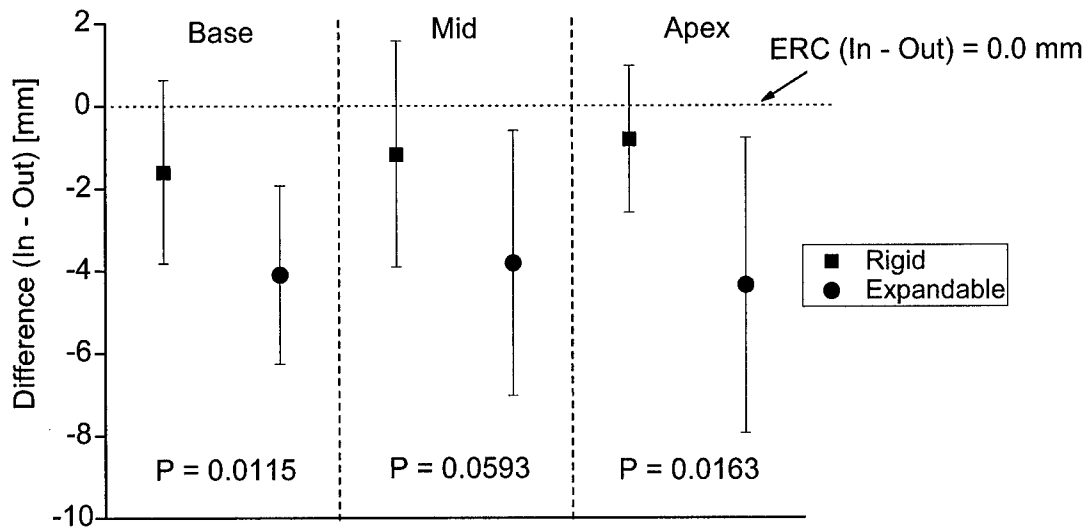
(a)
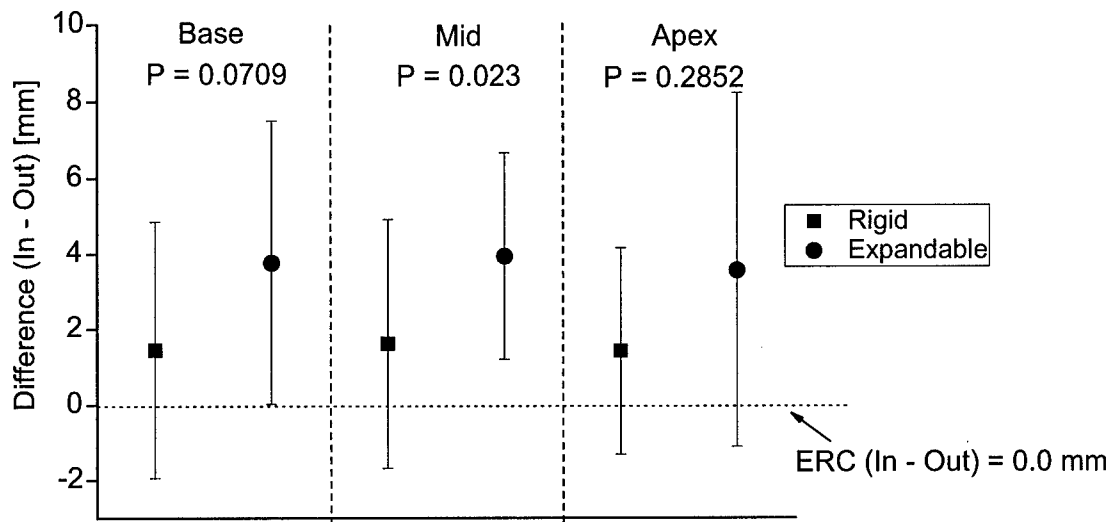
(b)

Figure 4. *Kim et al.,* Impact of endorectal coils on prostate distortion
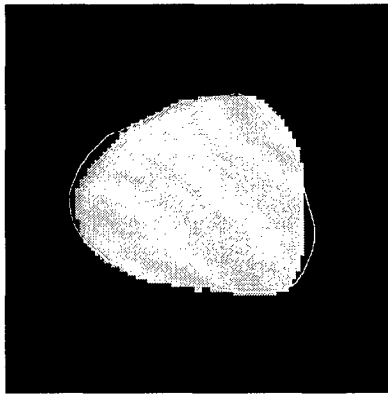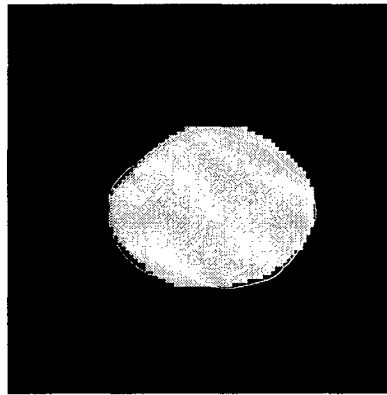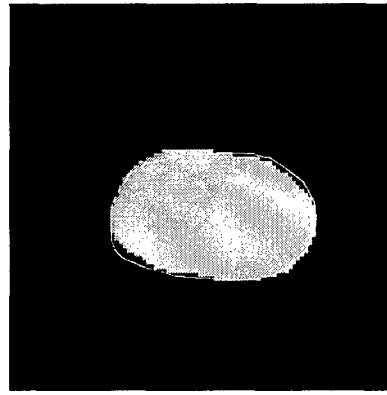
(a1)   (a2)   (a3)
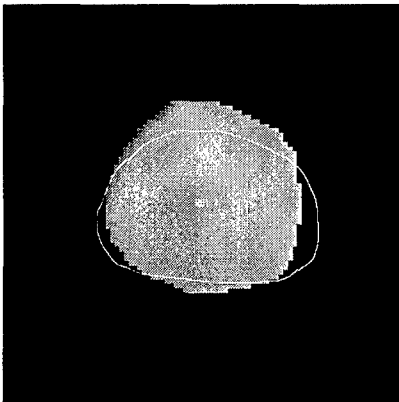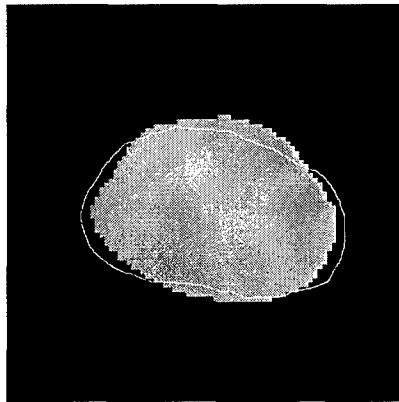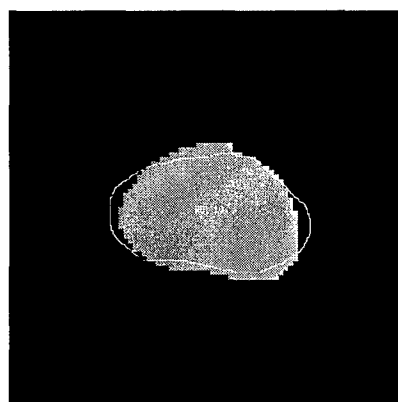
(b1)   (b2)   (b3)

Figure 5 *Kim et al.,* Impact of endorectal coils on prostate distortion
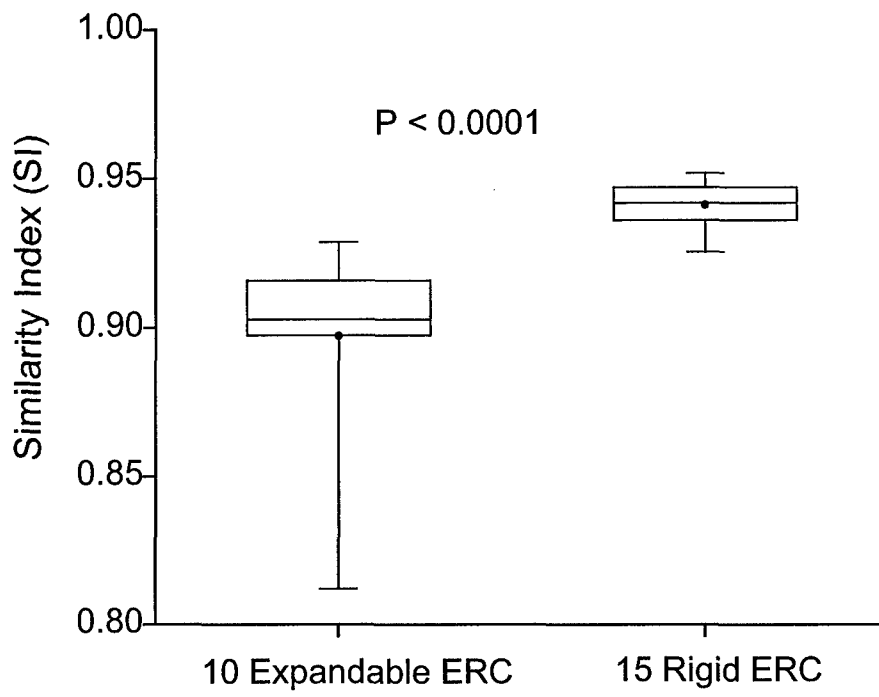
Figure 6. *Kim et al.,* Impact of endorectal coils on prostate distortion

Appendice

D Presentations to meetings

1- Yongbok Kim, Susan Moyher Noworolski, Jean Pouliot, I-Chow J. Hsu, and John Kurhanewicz, Analysis of prostate deformation due to different MRI/MRS endorectal coils for image fusion and brachytherapy treatment planning. Med. Phys.31 (6); 1728-1728, 2004 (Abstract).

2- Yongbok Kim, I-Chow Hsu, Etienne Lessard, John Kurhanewicz, Susan Moyher Noworolski, and Jean Pouliot, Dose Constraints in Inverse Planning HDR Prostate Brachytherapy for The Dose Escalation of DIL Defined by MR Spectroscopy Imaging. *Submitted for presentation at the 2005 Annual Meeting of the American Brachytherapy Society*, San Francisco.

-1-

Analysis of Prostate Deformation Due to Different MRI/MRS Endorectal Coils for Image Fusion and Brachytherapy Treatment Planning

Y Kim, S Noworolski, J Pouliot, I Hsu, J Kurhanewicz
University of California San Francisco, San Francisco, CA

Combined anatomic (MRI) and metabolic (MRSI) imaging is used to define the validated cancer lesion within the prostate for the dose escalation purpose. For the acquisition of high spatial resolution (~ 0.3 mm) spectroscopic imaging (MRSI) data, an endorectal coil (ERC) is mandatory. However, its presence causes distortions of the prostate and of the surrounding organs, making it difficult to use MRI/MRSI data directly for CT or MRI planning. In this study, the extent of the deformation of the prostate produced by the balloon ERC (five patients) versus the rigid ERC (fifteen patients) was measured to select which ERC should be used for the fusion of MRI/MRSI data with planning CT or MRI in high dose rate brachytherapy. ERC forces the prostate to tilt anteriorly with an average of
19.4 degree on sagittal view (19.5 and 19.2 degree for rigid and balloon ERC, respectively). The ERC compress the prostate in the antero-posterior (AP) direction with an average of 1.2 and 4.7 mm for rigid and balloon ERC, respectively. In the lateral direction, the prostate is widened with an average of 1.5 and 6.1 mm due to rigid and balloon ERC, correspondingly. In conclusion, the rigid ERC creates less deformation. The rigid ERC MR images can be aligned to MR images (no ERC) by manually rotating and translating the ERC MR images with a precision of 2 mm in the AP and lateral direction.

This abstract is presented at 46th Annual Meeting of American Association of Physicists in Medicine (AAPM), Pittsburgh, PA on July 25 - 29, 2004.

Kim Y, Noworolski S, Pouliot J, Hsu IC and Kurhanewicz J. Analysis of prostate deformation due to different MRI/MRS endorectal coils for image fusion and brachytherapy treatment planning. *Med. Phys.* 31(6), 1728 (2005)

Dose constraints in inverse planning HDR prostate brachytherapy for the dose escalation of DIL defined by MR spectroscopy imaging

Yongbok Kim, Ph.D.,1 I-Chow J Hsu, M.D.,1 Etienne Lessard, Ph.D.,1 John Kurhanewicz, Ph.D.,2 Susan Moyher Noworolski, Ph.D.,2 Jean Pouliot, Ph.D.1
1Radiation Oncology, University of California, San Francisco, San Francisco, CA;
2Radiology, University of California, San Francisco, San Francisco, CA.

Purpose: To obtain the dose constraint set (class solution) for the boost of dominant intraprostatic lesions (DILs) defined by MR spectroscopy imaging (MRSI) in HDR brachytherapy of the prostate cancer and the maximum achievable boost level under RTOG0321 dosimetric requirement.

Methods and Materials: For 10 patients (A to J), DILs were manually contoured on HDR planning CT/MR images based on combined MRI/MRSI. A lesion containing at least 3 contiguous MRSI validated cancer voxels was called DIL. The class solution of dose constraints, acceptable dose range and penalty values, were obtained from our previous clinical experience on inverse planning technique (IPSA). For each patient, six plans (a without-boost and 5 different levels of dose escalation to the DILs requesting a minimum of 110, 120, 130, 140 and 150% of the prescribed dose, respectively) were generated using IPSA. Dosimetric indices for each plan were computed and compared with the requirement of RTOG0321 protocol (V100 _90% for target coverage, V75 _1 cc for bladder and
rectum, and V125 _1 cc for urethra) to determine the acceptable level of dose escalation.

Results: Plans without boost satisfied all RTOG0321 requirements with average dose coverage of 92.1% to target (range from 90.6 to 93.8%). Four (B, C, D, and J) out of 10 patients prohibited any dose escalation whereas a certain level of boost to the DILs was feasible for the rest of patients, minimum dose of 110% for patient E, 120% for patient H and I, 140% for patient A and F, and 150% for patient G, respectively. The violation of RTOG0321 protocol is the rectal dose for 9 patients and the bladder dose for patient C. The average benefit from maximum achievable boost for 6 patients is 1.1% increase of target coverage and 5% increase of V120 dose to DILs compared with a plan without boost.

Conclusions: A certain level of dose escalation to DILs defined by MRI/MRSI is possible for some patients using class solution of IPSA under RTOG0321 dosimetric requirements depending on rectal and bladder dose.

This abstract is presented at 26th Annual Meeting of American Brachytherapy Society (ABS), San Francisco, CA on June 1 - 3, 2005.